Project Number: MQP-JNL-CNT9

Nano-Scale Convective Heat Transfer of Vertically Aligned Carbon Nanotube Arrays

A Major Qualifying Project Report

Submitted to the Faculty of the

WORCESTER POLYTECHNIC INSTITUTE

in partial fulfillment of the requirements for the

Degree of Bachelor of Science

in Mechanical Engineering

by

Alex Larsen

Ryan Whetstone

Date: 2010

_____

Approved:

Prof. Jianyu Liang, Major Advisor

Acknowledgments

We would like to thank all the members of the WPI Nanomaterials & Nanomanufacturing Laboratory (NNL) for all of their help and input with our project:

Nihar Pradhan

Qiming Yang

Yuqin Yao

Siddharth Meshram

Sara Gouveia

And our advisor Prof. Jianyu Liang

Abstract

The trend of miniaturization in electronics has led to much greater heat densities within computer chips, demanding high performance heat sinks at smaller and smaller scales. A vertically aligned array of carbon nanotubes could function analogously to a conventional fin or pillar heat sink. Using a nano-porous aluminum oxide template, aligned CNTs were grown by chemical vapor deposition, and processing parameters were varied for comparison. By applying a constant heat input, the steady state temperature was measured for different surface morphologies, enabling insight into nano-scale convection properties.

Introduction

Scientific investigation allows us to imagine, explore, and understand new realms of knowledge and possibilities for application. With the advancements in computer processing, microscopy, and micro-scale manufacturing, a previously inaccessible niche in science has opened at the most minuscule end of the size spectrum, known as nanotechnology. The "nano" in nanotechnology refers to the scale of a nanometer (nm), one billionth of a meter, but realistically, nanotechnology involves the development of materials and devices with distinct properties up to the hundred nanometer range. Figure 1 compares the scale of a multi-walled carbon nanotube (MWCNT) with other microscopic objects.

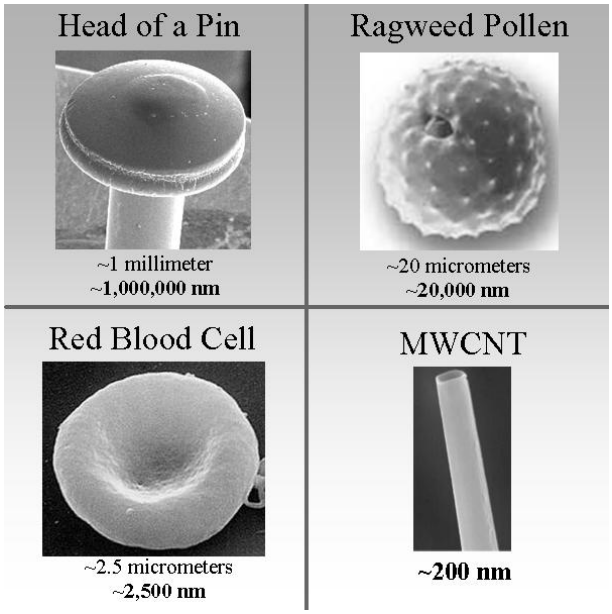

Figure 1: MWCNT scale compared to microscopic objects

Since the early 1990s, there has been a worldwide buzz surrounding nanotechnology, resulting in huge advances in its science and applications. Possibilities for manipulation of objects and creation of devices at the nano scale can be broken down into two categories, top-

down and bottom-up. Top-down strategies use macro-scale processes to affect nano-scale phenomenon, such as masked lithography, where an electron beam reacts with a sample in a controlled area based on the openings on a mask. Bottom-up strategies, responsible for many of the current nanomaterials, utilize material properties of self-assembly at the nano-scale to improve macro-scale properties.

Researchers within the Nanomaterials and Nanomanufacturing Laboratory at WPI have been growing carbon nanotubes in an anodized aluminum oxide template, which causes them to grow in vertical alignment. This bottom-up strategy produces a unique nanomaterial which has potential for application in many fields. As mechanical engineers, we began the project by immersing ourselves in the laboratory, working with the graduate students and our advisor Dr. Liang to learn the techniques and processes necessary to manufacture samples. After becoming oriented with the lab equipment and this specific area of study, a heat sink design process was chosen to investigate and determine the effects of nano-scale surface structures on convective heat transfer.

Background

It has been known for well over a century that carbon filaments will form when a carbon containing gas comes in contact with a hot metal surface. However, the discovery that the gas actually decomposes into carbon atoms then reforms into microscopic fibers was not possible until the development of high-resolution microscopes (Melechko 2005). Discernible images of carbon nanotubes (CNTs) were first published in 1952 by Russian scientists, but it was not until 1991 that Sumio Iijima discovered how to synthesize them. Since then, scientists around the world have explored new production methods, and their unique structure and symmetry have created much excitement surrounding their material properties.

Basics of CNTs

At the atomic scale, carbon can bond in multiple distinct crystalline structures, producing different allotropes, or structurally differentiated forms. Some allotropes of carbon include diamond, with a complex 3-D atomic structure (Figure 2a), graphite with a 2-D sheet of carbon atoms in a hexagonal array (Figure 2b), and amorphous carbon which has an unorganized crystal

structure (Thostenson 2001).

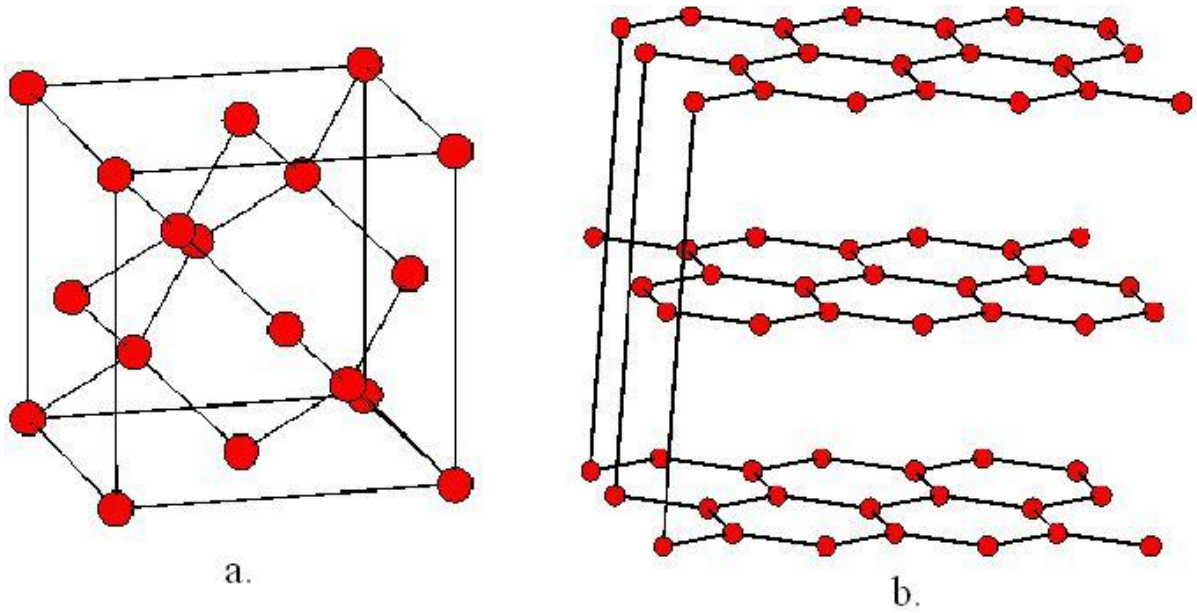

Figure 2: (a) diamond atomic structure (b) graphite atomic structure (EveryScience 2009)

Cylindrical allotropes of carbon can also form, where the atoms are bonded as if a graphite sheet, composed of hexagonal cells, were rolled into a tube. The bonding morphology of a CNT can have three known forms, armchair, zigzag, and chiral, based on the orientation of the horizontal cells (Figure 3).

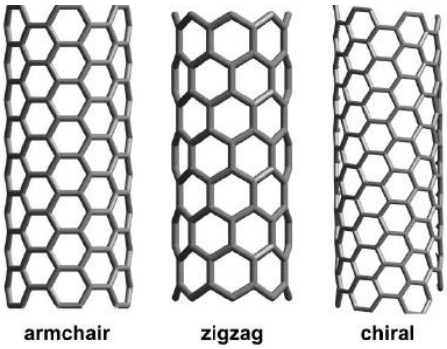

Figure 3: Three possible carbon nanotube atomic structures

CNTs can be divided into two main categories depending on the number of graphite layers in the tube. The smallest CNTs exist as one carbon layer cylinders, known as single-walled carbon nanotubes (SWCNTs), with very small diameters ranging from about 1-5 nm. There can also be CNTs nested within other CNTs, known as multi-walled carbon nanotubes (MWCNTs) with diameters up to 250 nm. The many concentric rings of CNTs closely spaced within a MWCNT are held together with relatively weak Van der Waals forces (Thostenson 2001). CNTs can be grown using multiple production methods, which has resulted in a plethora of CNT structures.

CNT Production Methods

Since the early 1990s, when Iijima first synthesized CNTs, three primary production methods have been developed: arc-discharge, laser ablation, and chemical vapor deposition. Based on the production method and the specific growth parameters, many different types of micro and nano scale carbon fibers have been produced, each with different structures and properties.

Arc-Discharge

The arc-discharge method is the original synthesis technique used by Iijima, and has proven to be the simplest process to date. The main components of this technique are two high-purity graphite rods, which act as an anode and a cathode. Under an inert atmosphere of helium, a voltage is applied between the rods until a stable arc is achieved. This electrical arc strips carbon atoms off the anode and deposits them on the cathode forming a build-up consisting of a hard carbon shell with a soft core containing CNTs and other carbon particles (Thostenson 2001). This process is shown below in Figure 4, and the resulting CNTs are shown in Figure 5.

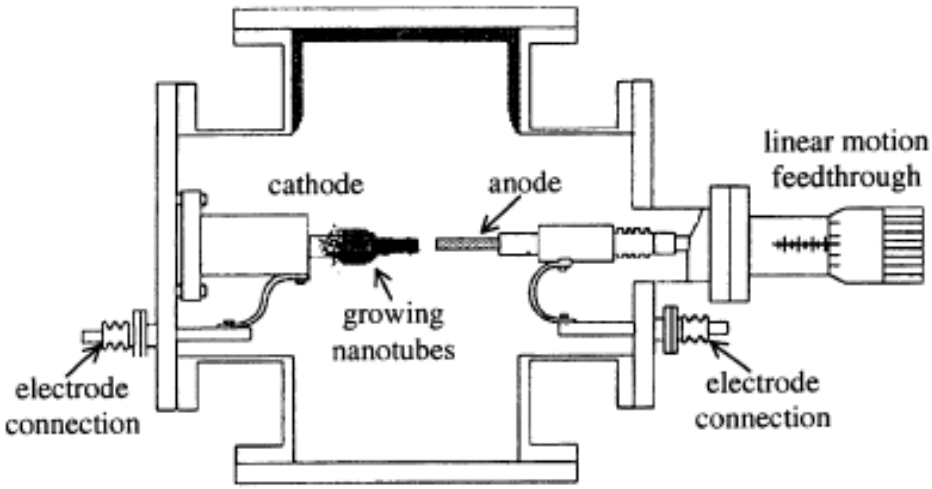

Figure 4: Schematic of arc-discharge process

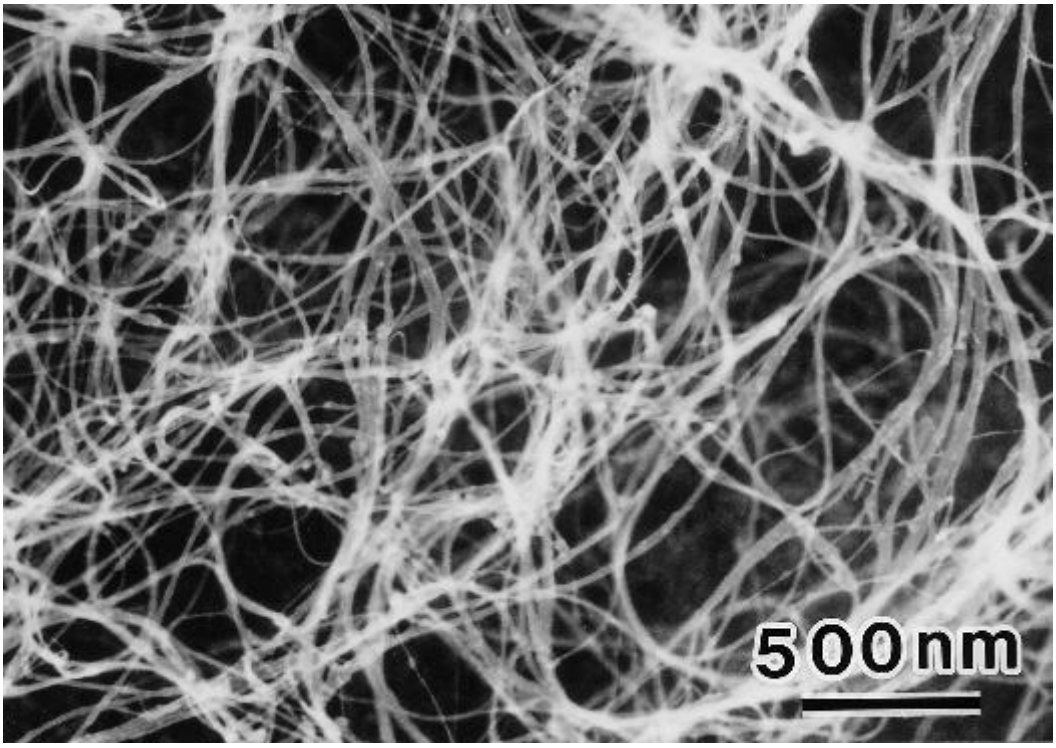

Figure 5: SEM image of carbon nanotubes produced by arc-discharge (Nano-labs.com)

Laser Ablation

The laser ablation technique was first used to produce fullerenes, another carbon allotrope similar to CNTs but with a spherical structure. Since the development of this method, it has been modified to allow for the synthesis of SWCNTs (Thostenson 2001). Graphite rods with a mixture of cobalt and nickel catalysts are put in a tube furnace with flowing argon gas. The vaporization of the graphite rod is achieved by applying two short laser pulses. The first pulse breaks the graphite rod into large particles and the second atomizes and deposits the carbon on the growing CNT. This process is shown below in Figure 6. This method results in a tangled mat of CNTs, similar to arc-discharge, but along with fullerenes and other junk carbon structures (Wilson 2002).

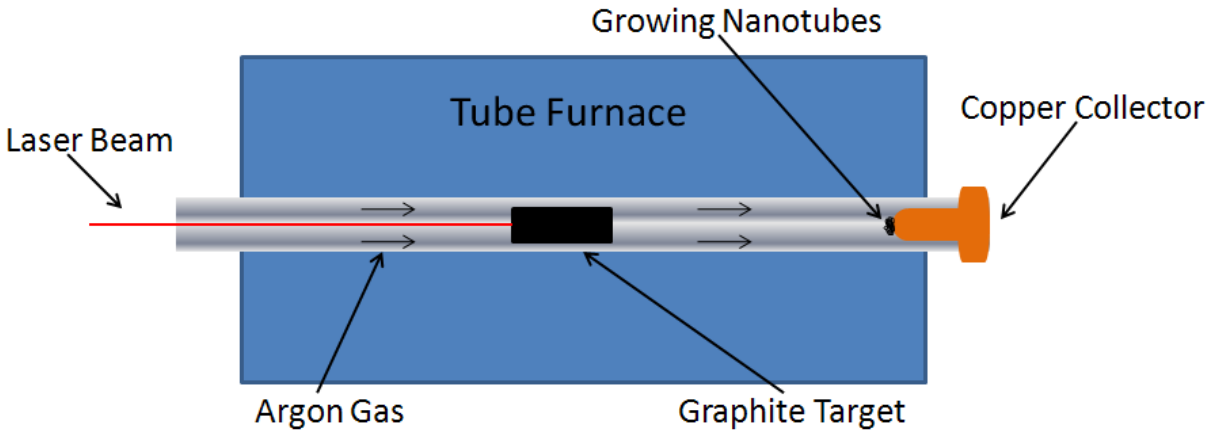

Figure 6: Schematic of the laser ablation process

Both the arc-discharge and laser ablation techniques suffer from the same primary drawbacks. First, they both involve vaporization of a single carbon source so only small quantities can be produced at a time. This makes it difficult for these methods to be scaled up for industrial applications (Thostenson 2001). The second drawback is that large amounts of junk carbon and undesirable nano-particles are mixed in with the tangled CNTs. Therefore, difficult purification steps are required in order to extract the CNTs for practical applications (Wilson 2002). These limitations led to the development of a new method called chemical vapor deposition (CVD).

Chemical Vapor Deposition (CVD)

In this process, nano-particles of a catalyst are deposited on a substrate surface before being inserted into a tube furnace. A carbon containing gas, such as acetylene then flows through the tube furnace at high temperatures, leading to decomposition of the gas into carbon atoms. The nano-particles of catalyst attract these carbon atoms, initiating CNT growth (Thostenson 2001). This process is illustrated in Figure 7.

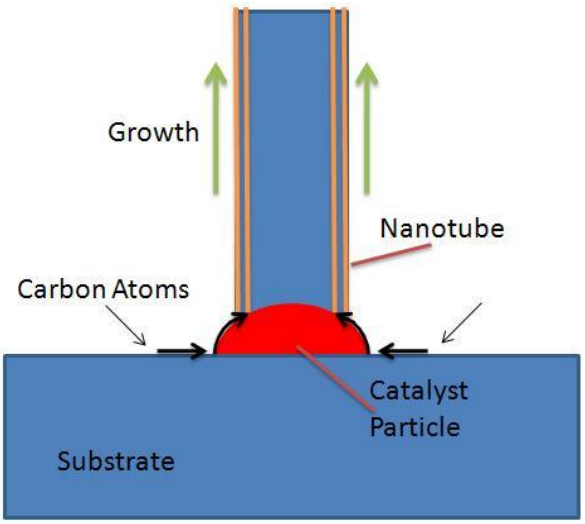

Figure 7: Catalyst initiation and growth of carbon nanotubes

By using lithography techniques, a mask can be produced which allows for controlled size and spacing of the catalyst deposition. Although limited alignment has been observed due to van der Waal interactions between neighboring CNTs, the result of basic CVD is still generally a tangled mat of CNTs (Melechko 2005). It was not until the development of plasma enhanced chemical vapor deposition (PECVD) that true vertical alignment of CNTs was achieved.

PECVD is similar to CVD since the deposition of a nano-particle of catalyst is required to begin CNT growth. The primary difference between these methods is that during CVD, vaporization of the carbon gas occurs via thermal energy only, while in PECVD a voltage is applied during the growth process. This causes current flow through a plasma medium within the furnace tube, bombarding the carbon gas electrons. This electrical energy input reduces the activation energy for CNT growth, and therefore decreases the process temperature required for the reaction. The most important, albeit unexpected benefit of PECVD is the vertical alignment caused by interactions with the electric field. This field causes each CNT to grow almost completely vertical, minimizing entanglement with its neighbors as seen in Figure 8 (Melechko 2005).

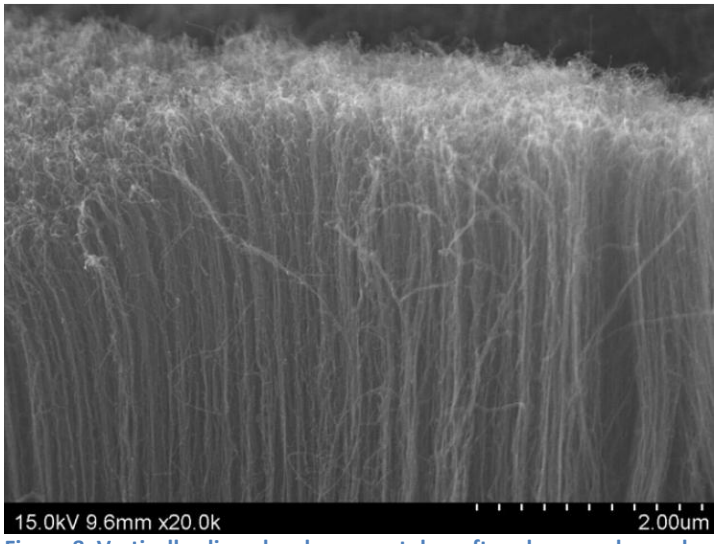

Figure 8: Vertically aligned carbon nanotubes after plasma enhanced chemical vapor deposition (Shaikh 2007)

Another CVD method which results in vertically aligned CNTs uses a specialized material with closely packed nano-diameter pores as a template. Materials such as anodized aluminum oxide (AAO) have a high density of vertical nanopores, which extend completely through the ceramic matrix. Through CVD, carbon atoms can be deposited on the inside walls of these nanopores to form MWCNTs, in some cases even without a catalyst. The resulting CNTs are many layers thick and are vertical since they follow the direction of the pores. This vertical alignment is desirable for many applications.

These three basic categories of production have diversified into hundreds of specific, highly deterministic modes of CNT synthesis, which means the position, alignment, diameter,

length, and chemical composition of individual nanostructures can be manipulated (Melechko 2005). This evolution has enabled production of CNTs with unprecedented material properties.

Material Properties of CNTs

CNTs have been shown to have incredible mechanical, electrical, and thermal properties, some of which have been reported to exceed any other known material. Despite the amazing properties of CNTs already witnessed, very few have reached the theoretical predictions calculated for idealized CNT structures. This means more work is required in optimizing production methods, in order to limit the defects and resistances which lead to the less than anticipated results (Thostenson 2001).

Scientific interest in CNTs was first sparked by the discovery that they possess remarkable mechanical properties. In macro-scale structural materials, there is always a trade-off between strength and ductility, with strong materials tending to be brittle, and ductile materials tending to be weak. CNTs have been shown to have remarkably high strength, stiffness, fracture resistance, and elastic modulus, while still maintaining significant flexibility and ductility in the sense that they can withstand high longitudinal strain and bending moments. In the axial direction, MWCNTs are one of the strongest and stiffest known materials, with a measured tensile strength and elastic modulus of 150 GPa and 900 GPa, respectively, versus about 0.65 - 3 GPa and 200 GPa for stainless steel (Demczyk 2002). In other words, CNTs are over 100 times stronger than steel at only a minuscule fraction of its weight. In contrast to CNTs high tensile strength, they tend to buckle easily under compression as a result of their large aspect ratio.

CNTs are also attributed with having excellent thermal and electrical conductivity in the axial direction. Due to the unique structure of CNTs with the 'armchair' morphology, superb electrical properties are believed to exist. Theoretical calculations of electrical current density range from 10^9 to 10^{13} A/cm^2, and experimentally a SWCNT has been measured to be 10^7 A/cm^2, about 100 times greater than copper (Hong 2007). All CNTs are expected to be very good thermal conductors exhibiting a property called ballistic conduction, defined as the unimpeded flow of heat phonons through a material.

For a single discreet MWCNT, thermal conduction has already been measured to be about 3000 W/mK, only half its theoretical prediction (Kim 2001). Experimental testing of CNTs has resulted in a wide range of measurements which rarely correlate with their theoretical

estimation. There are many possible explanations for this observed range, such as defects from the manufacturing process, and non-comparable testing procedures. For instance many testing methods use 'mats' of aligned CNTs, and interpolate their results for a single tube. This method has proven to be inaccurate since large resistances exist between neighboring tubes. Recent experiments using isolated CNTs have resulted in more accurate measurements, but additional research is still required.

Applications of CNTs

The size and properties of CNTs have resulted in thousands of proposed applications which could revolutionize a wide range of fields. Already, some incredible applications have been realized by utilizing their unique mechanical, electrical and thermal properties.

CNTs' high tensile strength and stiffness allows for many potential applications. If CNTs are woven into a fabric they can be used as stab proof and bullet proof combat jackets. The high tensile strength may eventually allow CNTs to replace steel in many applications such as the cables on suspension bridges and the reinforcement bars in concrete. If tensile strength can be increased further, it may allow for the development of a space elevator. This project proposes to create a tether between the earth and a space station which can transport supplies and personnel (LiftPort 2009).

The unique network of carbon-carbon bonds which make up the CNTs leads to excellent electrical properties which may one day lay the groundwork for micro and nano-scale electronic devices. One of the most promising electrical applications are tiny interconnects between miniature electronic devices. The high thermal stability and most importantly the extremely large current carrying capacity, allow for performance comparable and even surpassing current macro-scale copper interconnects (Naeemi 2007). Mixing CNTs into various matrixes creates advanced composites which can have enhanced or additional properties. For example plastics are typically electrical insulators, but when a small amount of CNTs are evenly dispersed they can become conductors (Jimenez 2007).

CNTs also present potential for thermal applications, since they are one of the only known materials which exhibit a phenomenon known as ballistic conduction, where units of heat called phonons travel through the structure virtually unimpeded. One idea is that CNTs could someday be used to destroy cancer cells by thermally activating them within a tumor using radio

waves. While this type of application is still years from being realized, the thermal properties of CNTs can be useful for the performance enhancement and miniaturization of heat sinks, which act to dissipate heat as quickly as possible from a thermal system.

Heat Sink Design: Present and Future

Modern heat sinks usually consist of an array of thermally conductive metal pillars or fins which are connected to a heat source. To remove heat, a fluid is directed through a heat sink structure and heat dissipates as it flows over the surface. This form of heat transfer between a solid surface and a surrounding fluid is called convection. Maximizing the convective heat transfer between a heat sink and the fluid is critical and will be a key challenge in the miniaturization of electronics.

Heat Sink Design Overview

A heat sink's effectiveness depends on the thermal interface between the heat source and the heat sink, the thermal properties of the material used, and the shape of the heat sink. A general heat sink schematic is shown below in Figure 9.

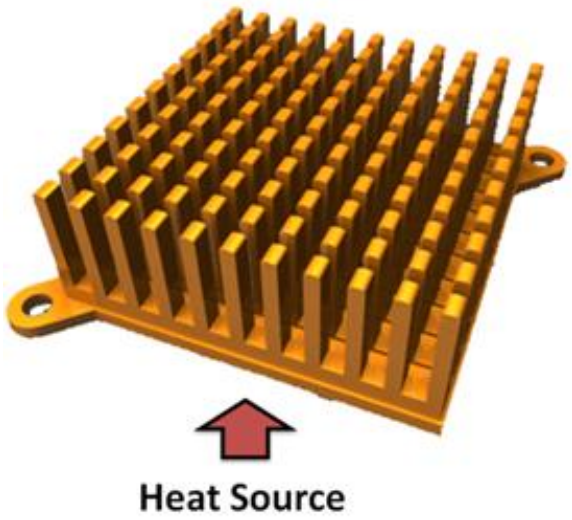

Figure 9: Basic heat sink design

The connection between a heat source and the bottom of a heat sink is known as a thermal interface. Good thermal conductivity is needed at the thermal interface for heat to flow efficiently from the heat source to the heat sink. Maximized physical contact between the surfaces is also critical, but even the flattest surfaces encountered only make true molecular contact at 1-2% of the surface area (Garimella 2006). This issue is addressed by using a thermal interface material (TIM) to mate the two surfaces on the molecular level. Silicon-based thermal grease and powdered silver paste are two commonly used TIMs, with thermal conductivities of 1-3 and 8 W/mK, respectively. These thermally conductive, viscous, liquids displace the thermally non-conductive air (0.024 W/mK) which would normally occupy the empty spaces between the surfaces (Conway 2006).

Optimized thermal interfaces with minimum thermal resistance are necessary for maximized heat sink performance.

Once heat has crossed the thermal interface, the heat sink material should be able to transport heat away from the source as quickly as possible. The free electrons in many metals give them very high thermal conductivity. Aluminum (≈ 250 W/mK) and copper (≈ 400 W/mK) are the most commonly used materials for heat sink structures. Due to fast heat flow, low material cost, and relatively easy processing, these two metals are ideal for commercial use in today's computers. However, as electronics become more miniaturized, new materials and methods will be required to dissipate heat at much smaller scales.

The amount of thermal transport that takes place also depends on the shape of a heat sink. High surface area is desirable to maximize contact between the heat sink and the fluid; hence the use of many pillars or fins. The aerodynamic characteristics along the axis of flow are also important. Various shapes and designs have been explored and improved upon for the purpose of maintaining the coolest possible temperature in a computer's central processing unit (CPU). Figure 10 shows the leap in CPU heat sink design from 1992 to 2007, with shape as the major design variable.

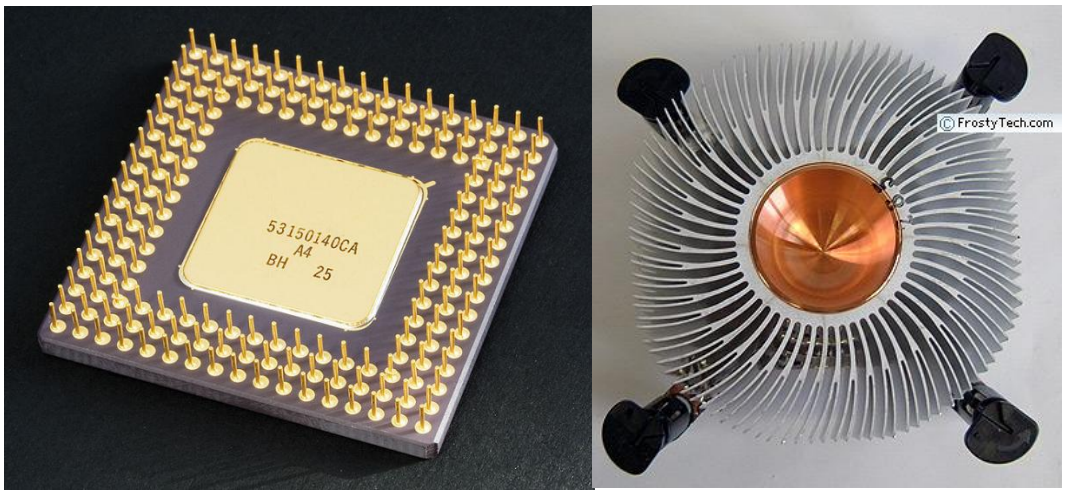

Figure 10: Progression of Intel heat sink design from 1992 to 2007 (Page 2009)

Over the last decade, smaller and more powerful processors have been evolving, with continually rising power densities within the chips. This has caused increased heat output, driving the progression in heat sink design. As the scale of computing continues to decrease, new

designs are beginning to explore micro and nano scale heat sink applications. Noteworthy engineering strategies for micro heat sink design are discussed in the next section.

Micro Heat Sink Design Strategies

When designing a micro heat sink, the limiting factors in performance are still the thermal resistance of the thermal interface, the conductive structures, and the convective structures (Varanasi 2008). Various new nano and micro scale materials and processes have been shown to lower thermal resistance at these interfaces compared with their macro scale analogues.

According to Ravi Prasher, an editor for the Institute of Electronics and Electronics Engineers, the "use of nanoparticles or nanotubes are almost inevitable for the future miniaturization of thermal interface materials" (Prasher 2006). Mixing randomly oriented MWCNTs into a conventional thermal interface material has been shown to increase thermal conductivity of the bulk material (Thang 2009). MWCNTs have been grown in vertically aligned arrays and coated with copper to aid in heat transfer, which was then partially etched away to expose MWCNT pillars, but these samples showed thermal resistance comparable to commercial silver paste, about 50 mm^2K/W (Ngo 2004, Li 2007). Still, these studies show that vertically aligned MWCNTs can accomplish increased heat conduction via increased surface area for heat transfer. This concept has also been tested simply using PECVD to grow vertically aligned SWCNTs directly onto aluminum, showing improvement with a much lower thermal resistance (Zhang 2008). This makes sense because SWCNTs are known to have a higher thermal conductivity than MWCNTS, and there are likely an increased number of contact points made by the smaller SWCNTs. For micro/nano-engineered thermal interface materials to truly surpass conventional thermal compounds, even lower thermal resistance will be required (Prasher 2006).

Thermal conduction at this scale has also been engineered using unique new material manipulations and processes. Thermal management systems have been integrated into some of the smallest computer chips possible today. Silicon, an easily micro-machined material was used for a multilayer thermally conductive micro-chip. For maximum thermally conductive contact, the silicon was selectively etched to remove only certain crystallization layers, enabling the chip to maintain operating temperature at a heat flux of 100 W/cm^2 (Pilchowski 2000). CNTs are another nano-engineered material known to have substantial thermal conductivity, and their potential for one-dimensional thermal transport is desirable. The conductivity of materials used

for micro heat sink applications is important to design, but future research "should also focus on minimizing the total thermal resistance rather than just increasing the thermal conductivity" (Prasher 2006).

This drop in total thermal resistance of a system can be reduced by maximizing micro and nano scale convective heat transfer, especially as the size of the chips continue to decrease. A variety of techniques have been used for this purpose, including nanofluids, micro-channels, "heat pipes", and unique surface structures. Nano-fluids contain extremely small metal or ceramic particles (10 - 100 nm) to create a fluid with enhanced thermal properties (Patel 2005). Micro-channels have been incorporated into metals and ceramics with diameters as low as 250 µm. Fluid can then be pumped through these systems, resulting in rapid heat transfer. Phase change cycles can also be utilized in microscopic heat pipes, where evaporation of the convective fluid allows it to pass through a nanoporous membrane and condense on the other side. This is analogous to the cooling effects of sweating, but controlled by nanopores instead of sweat glands (Vasiliev 2008).

Micro and nano-scale surface structures can also be used to increase convection by increasing the total surface area available for heat transfer. Metallic rods averaging 10 µm long and 2 µm wide were grown on a copper substrate to test their convective cooling properties. In order of performance, nickel, silver, and copper micro-rods were shown to lower the steady state temperature for a micro-chip with constant heat output (Son 2004). Though the rods were shown to increase heat transfer compared to the copper substrate, the power handling capacity of this device was too low for today's computers. Further investigation into the effect of surface structure on aerodynamics and heat transfer at this scale has applications in future microelectronic heat sink designs. Even smaller heat sink fins with good thermal conductivity could be manufactured and tested using aligned MWCNTs.

Potential for Aligned MWCNT Heat Sink

MWCNTs are a potential material for a heat sink due to their cylindrical structure, high axial thermal conductivity, and ability to be manufactured in a vertically aligned array. MWCNTs have been used in an aligned bulk mass to create a micro-scale heat sink (Figure 11), showing a 1 mm x 1 mm heated area topped with 10 x 10, 1.2 mm long aligned MWCNT bundles.

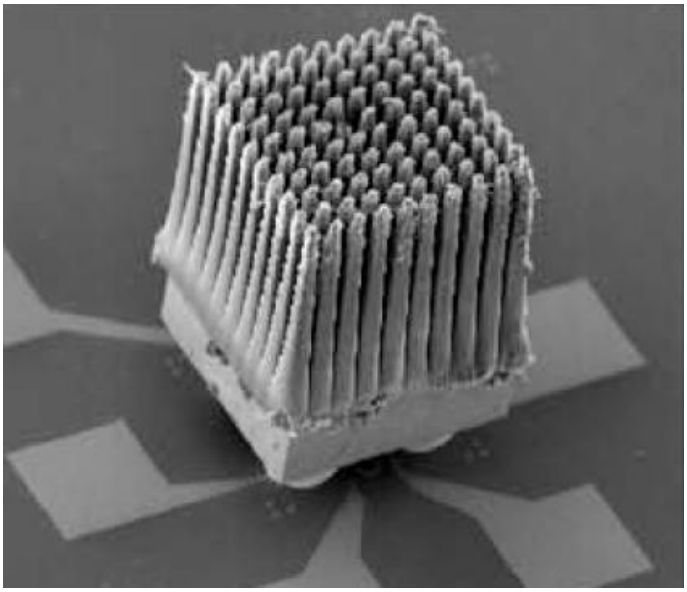

Figure 11: Micro scale heat sink design using MWCNT bundles

This heat sink design showed approximately equal performance compared with a 10 x 10 copper fin structure of the same size. To improve performance, the fin size should be made even smaller, so there is even more surface area for heat transfer, and the CNT-CNT interfacial resistance must be minimized (Kordas 2007). Mixed into silver paste, MWCNTs have been shown to improve thermal dissipation in a convective heat sink application (Thang 2009). However, aligned arrays of CNTs have shown improved thermal conductivity versus randomly dispersed CNTs (Pradhan 2008). An example of a vertically aligned MWCNT array which could be used as a heat sink is shown in Figure 12.

Investigating the convective properties of an aligned array of MWCNT pillars is an opportunity to gain insight into the science of nano-scale convection. Based on this knowledge, we have determined that the convective properties of such an array should be explored, an optimized surface structure should be designed, and an experimental set-up should be developed for testing.

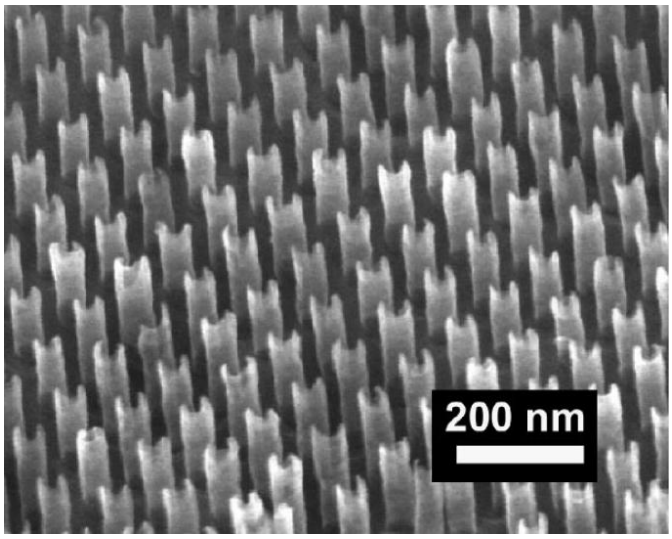

Figure 12: SEM image of vertically aligned carbon nanotubes grown in AAO template (Melecho 2005)

Design and Construction

To produce a vertically aligned array of MWCNT pillars with potential as a heat sink, four manufacturing steps must be performed: anodization to create a nanoporous AAO template, template assisted chemical vapor deposition of MWCNTs, oxidation of excess surface carbon

(a.k.a. thermocleaning), and chemical etching of the alumina to expose the tips of the MWCNTs. The entire process is shown in Figure 13, followed by a description of each step.

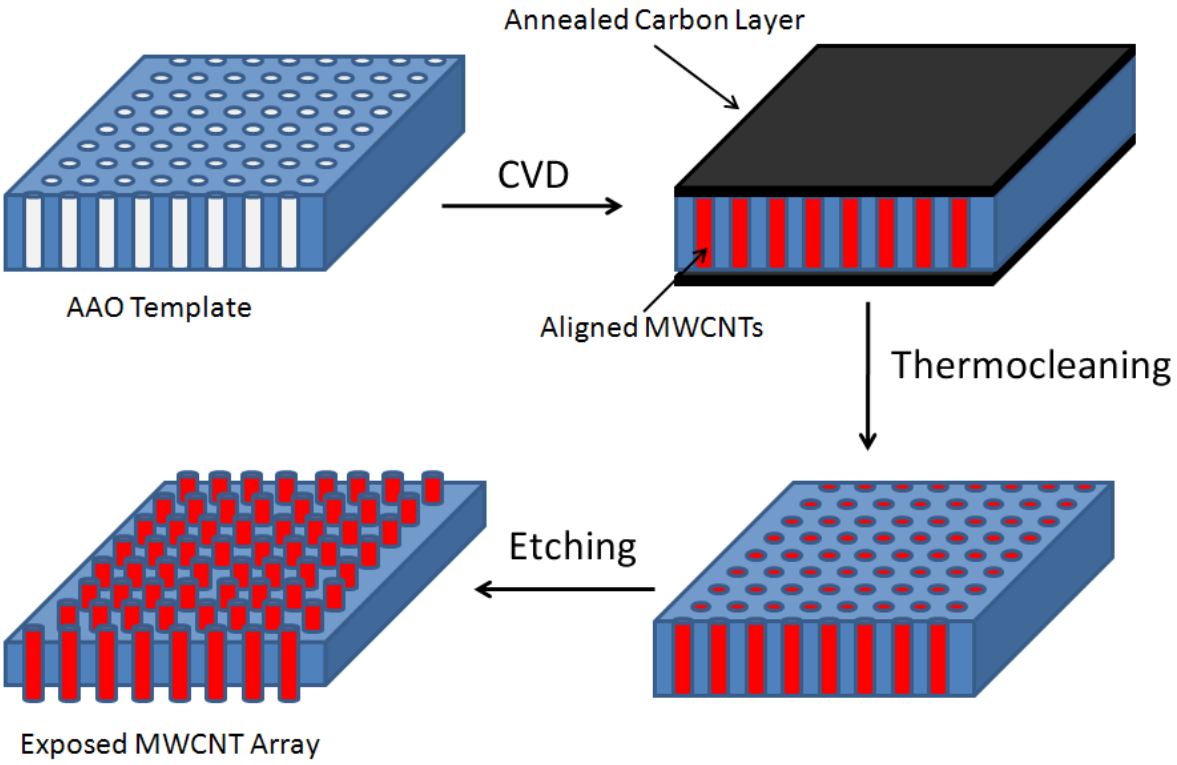

Figure 13: Sample production process

Anodized Aluminum Oxide (AAO) Template Anodization:

Aluminum anodization is the process which produces a nanoporous aluminum oxide layer on an aluminum substrate when it is submerged in an acid solution and subjected to a voltage. Aluminum anodization has been used to improve corrosion resistance for many years, but recently it has become important in nanotechnology. The combination of acid and applied voltage changes the aluminum surface into an aluminum oxide layer with a self-ordered array of nanopores, shown in Figure 14. The hexagonal pattern of nanopores observed in AAO templates has recently been explained using an ionic nano-convection model, wherein it was shown that convection is likely responsible for the initial charge distribution which gives rise to the beginnings of the nanopores. As the anodization process continues, the pores propagate through the layer. Once anodization is complete, this layer can be removed in order to expose the bottom side of the porous membrane, producing a blank AAO template (Lu 2009).

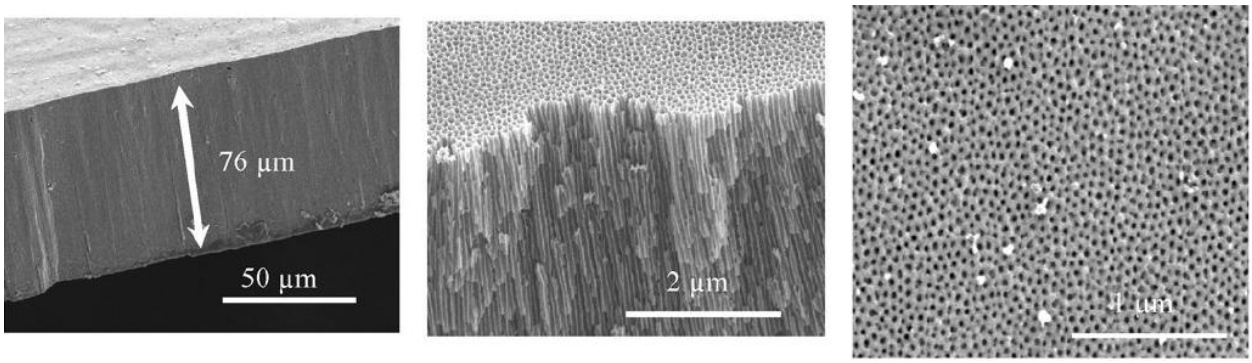

Figure 14: Three angles of SEM imaging showing the morphology of anodized aluminum oxide

Pore size and inter-pore distance increase with increased voltage, and different acids can be used, which yield slightly different results (Belkarwar 2009). Though these parameters may have some effect on the eventual sample's convective properties, for our purpose, commercially produced AAO templates are the best choice. They are consistent and readily available, and the parameters for MWCNT growth on these templates are already known for the systems we have available for manufacturing.

Template Assisted MWCNT Growth:

Researchers in the Nanomaterials and Nanomanufacturing Laboratory at WPI have developed a procedure for template assisted chemical vapor deposition of MWCNTs into an anodized aluminum oxide matrix. Process parameters have been determined which result in consistent MWCNT growth using the setup shown below in Figure 15.

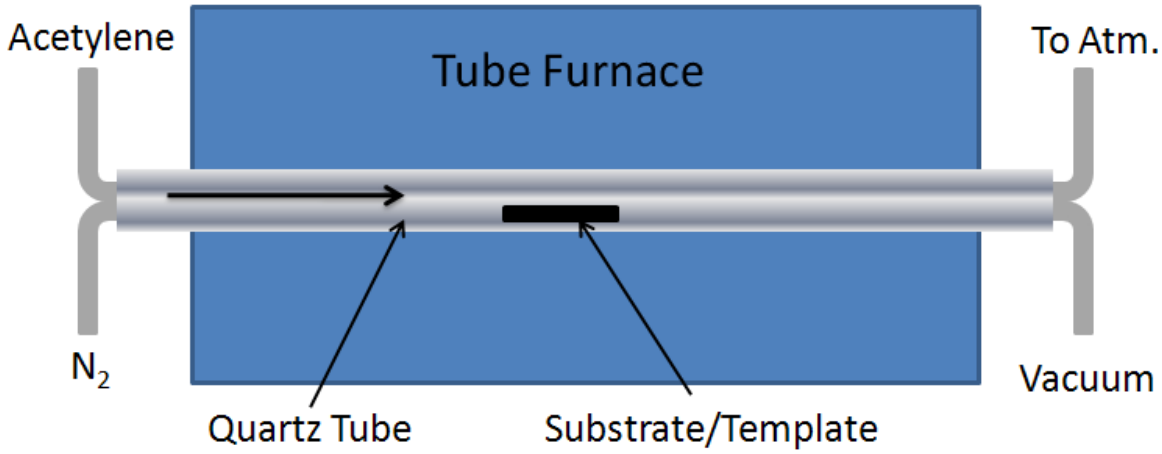

Figure 15: Schematic of template assisted chemical vapor deposition process

AAO templates are heated in a tube furnace to 700ºC with nitrogen flow at atmospheric pressure. Once heated, the carbon containing gas acetylene (H-C≡C-H) is introduced into the tube environment at a controlled concentration relative to the nitrogen flow. Due to the intense heat at the center of the tube, the acetylene vaporizes, and the released carbon atoms arrange into MWCNTs within the AAO nanopores. By varying the time and concentration of the acetylene flow, the thickness of the MWCNTs can be controlled. Unlike traditional CVD processes, an additional catalyst does not need to be added because the AAO template can initiate CNT growth itself. After the desired amount of time, the acetylene is turned off, and the samples anneal at 700ºC for an additional 12 hours under continuous nitrogen flow. The ideal furnace temperature, concentration, time of acetylene flow, and annealing time have all been previously determined, and these parameters will be used for manufacturing all of our testing samples, further described in the methodology section.

Thermocleaning

After CVD, the sample is blanketed with clumps of foam-like amorphous carbon, which can easily be removed using tweezers for large pieces, and a paper towel for small pieces. SEM imaging of the sample at this point shows that there is a patterned three dimensional annealed carbon layer bonded to the top of the MWCNTs at the template surface, shown below in Figure 16.

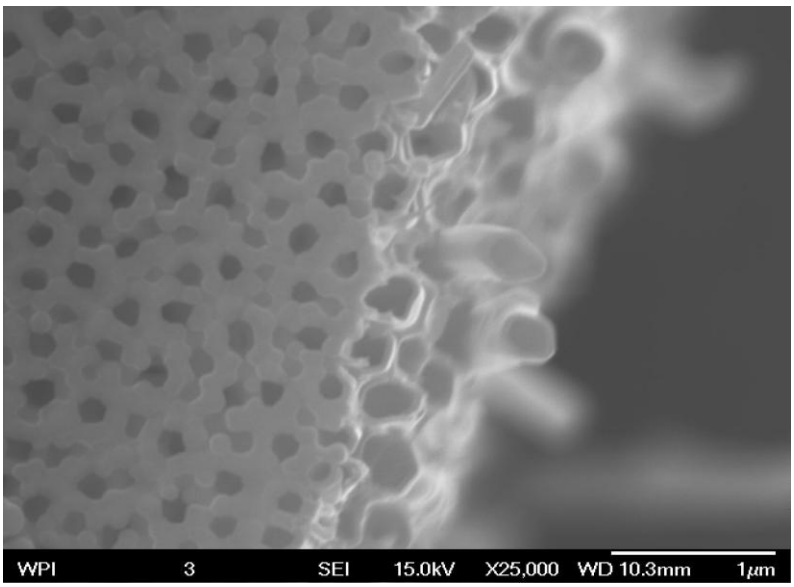

Figure 16: Annealed carbon layer with some exposed carbon nanotubes on the right

Thermocleaning is used to expose the MWCNTs by removing the annealed carbon layer via oxidation in a high temperature air filled furnace. It has been shown to burn off at a temperature of 650°C, consistent with a crystalline, graphite-like structure (Xiaowei 2004).

Figure 17 below shows the top surface of a sample after thermocleaning at 650°C for 15, 20, and 30 minutes. These images show the progression of oxidation over time, slowly removing the annealed carbon and exposing the template. At 20 minutes, the layer has almost been completely removed, and at 30 minutes, the whole layer has been oxidized, along with the CNTs underneath. Therefore, the time required to completely remove this layer while leaving the CNTs intact should be between 20 and 30 minutes. Optimization of this parameter is required to complete the heat sink design.

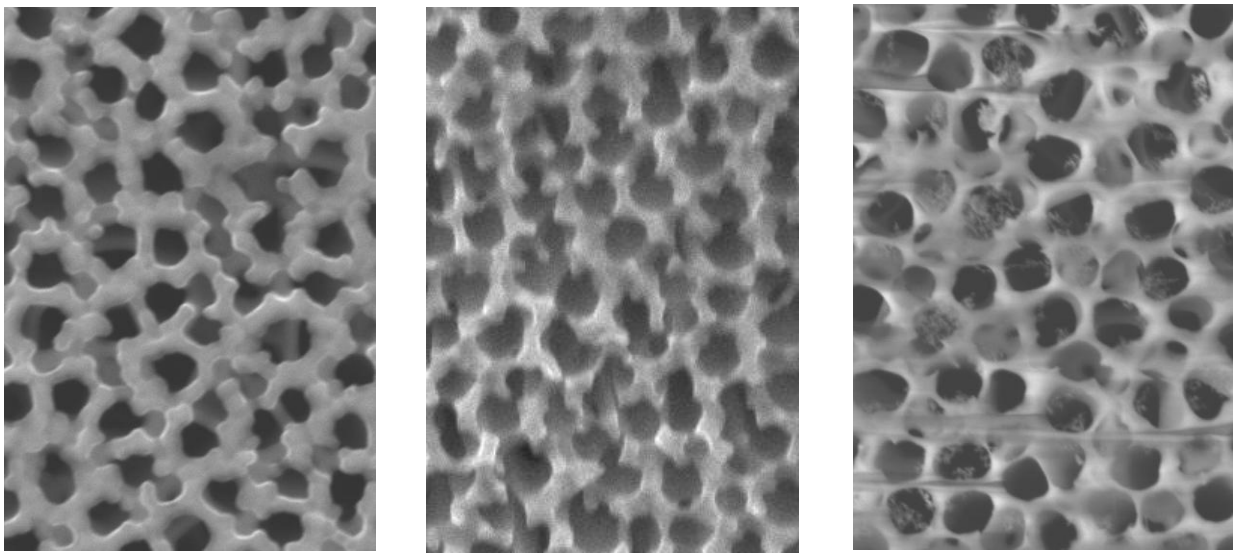

Figure 17: Incremental thermocleaning showing the removal of the annealed carbon layer at 15 min, 20 min, and 30min

Etching

Once the annealed carbon layer is removed by thermocleaning, the surface of the AAO template is exposed, with MWCNTs filling all the nanopores. In order to expose the tips of the MWCNTs, a wet etching process can be used to dissolve the AAO substrate at the surface. The acidic etching solution reacts with the surface molecules at a constant rate which results in linear mass loss (Hu 2009). CNT protrusion length can be controlled by knowing the etching rate of a particular acid and varying the etching time.

The most common etchant of AAO template is NaOH, however this acid results in rapid non-uniform removal of surface material. In order to produce protrusions which will not clump together, a very thin layer of material must be removed evenly over the entire surface. A much milder etchant is phosphoric acid (H_3PO_4) which reacts at a much slower rate and allows for a larger amount of control (Hu 2009). The etching rate can be further controlled by varying the concentration of the H_3PO_4 solution. High concentrations of H_3PO_4 such as a 10 wt% solution have a much faster etching rate than a 3 wt% solution (Hu 2009).

To produce an array of MWCNT protrusions with a controlled aspect ratio without clumping, a mild etchant must be used for a relatively short amount of time. To ensure that the length of CNT protrusion is consistent over the entire sample a low concentration of H_3PO_4 such as 3 wt% is ideal. To determine the etching time that results in this ideal protrusion length, a parallel etching optimization process could be performed.

Imaging and Testing Methods

Creating an aligned MWCNT array heat sink demands sample imaging at extremely small scales to collect data for the design optimization process. Logical and measurable testing methods are necessary to measure the comparative effectiveness of a nano-scale heat sink.

Scanning Electron Microscope Imaging

The scanning electron microscope (SEM) has proven to be one of the most useful pieces of equipment in a wide range of fields from biology to material science. The SEM is different from conventional light microscopes, because electrons are used instead of photons. Since the wavelength of an electron is significantly smaller, the SEM produces images with incredible resolution. This means features spaced as close as 1-5 nm can still be distinguished separately. In addition, SEMs have a very large depth of field which allows a large portion of the sample to be in view at the same time.

The SEM image is generated by the interaction of electrons with the atoms on the sample surface. The resulting deflections produce signals which contain information about the samples topography and composition (Klesel 2009). The electron beam is generated by the electron gun, which is typically composed of a tungsten cathode. A voltage is applied to the cathode which causes the electrons to move towards the positively charged anode and down to the sample.

Before this beam reaches the sample it must be condensed and focused by magnetic lenses into a very fine point. A final lens deflects this beam back and forth in a raster scan so the entire frame can be viewed at once (Klesel 2009). Figure 18 shows the major components of a scanning electron microscope.

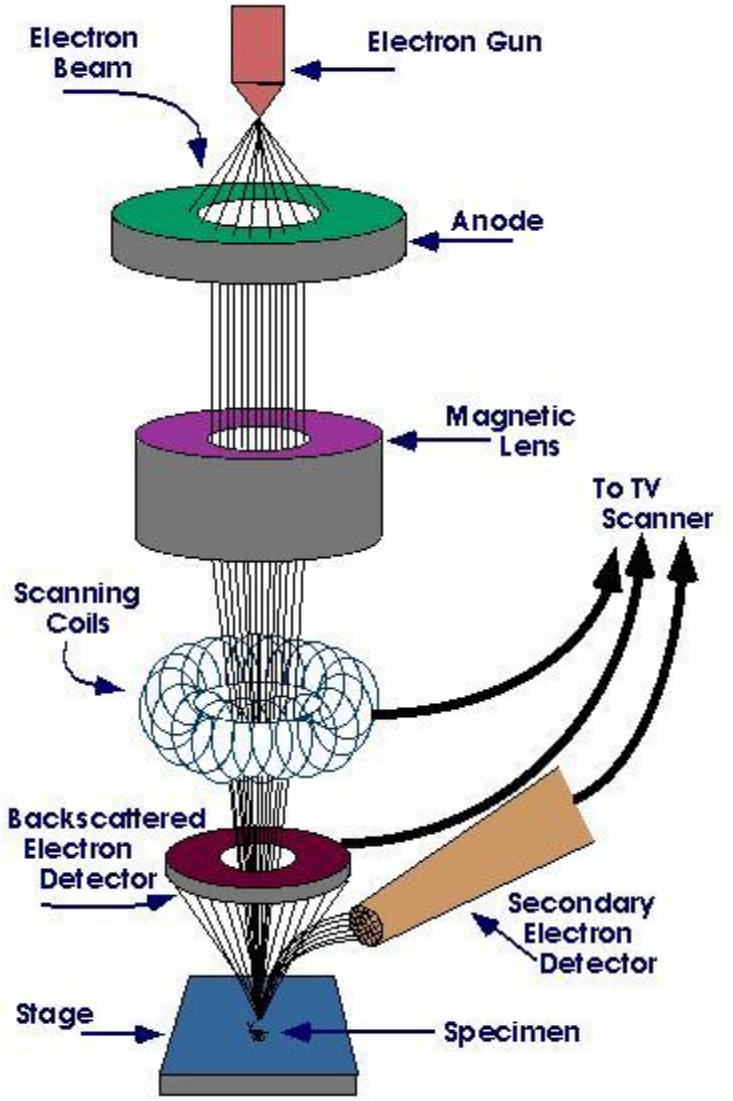

Figure 18: Major components of a scanning electron microscope

varying shades from white to black corresponding to different elements.

There are two conditions that must be satisfied in order to produce a clear and readable

When the electrons strike the sample, they are scattered and absorbed within a teardrop shaped interaction volume which extends about 100 nm to 5 µm into the surface. The electron deflections from both elastic and inelastic scattering result in a variety of interactions, the most useful being secondary electrons and back-scattered electrons, see Figure 19.

Secondary electrons originate from within a few nanometers of the surface, and the number of electrons detected depends strongly of the angle of the surface features. Since steep edges appear brighter, clear 3-D topographical images can be produced (Goldstein 1981). Back-scattered electrons originate from deeper in the surface and the amount deflected depends on the atomic weight of the elements in the sample. The result of this technique is an image with

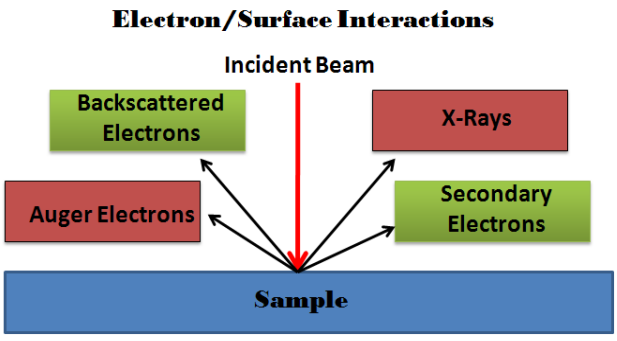

Figure 19: Electron surface interactions

image. First, the chamber from the electron source to the sample must be kept at a vacuum, primarily to eliminate interactions between electrons and any gas particles which would destabilize the beam. The other critical condition is that the sample surface must be electrically conductive and grounded to prevent the accumulation of an electrostatic charge. If the sample is not conductive already, a process called sputter coating can be used which deposits an ultrathin coating of highly conductive metal to allow imaging (Klesel 2009).

SEM imaging is a crucial technique for our project since we need to examine surface structure morphology at such small scales. Optimization of our manufacturing parameters will require extensive SEM observations. Once the nano-scale surface morphology of each sample is known, a comparative testing method can be performed.

Comparative Testing Method

Obtaining quantitative results for a nano-scale surface structure's convective properties requires macro-scale measurement devices to be used in order to detect nano-scale phenomenon. This presents a unique problem to scientists studying these systems. Concrete, accurate values for material properties at the nano-scale are inherently difficult to verify with high certainty, so comparative methods become a good way to acquire data with which to analyze nano-scale systems. For our testing, tiny thermistors are used to record temperature measurements over time. Under constant heating, we can obtain data for varied surface morphology, enabling comparative analysis of the convective properties.

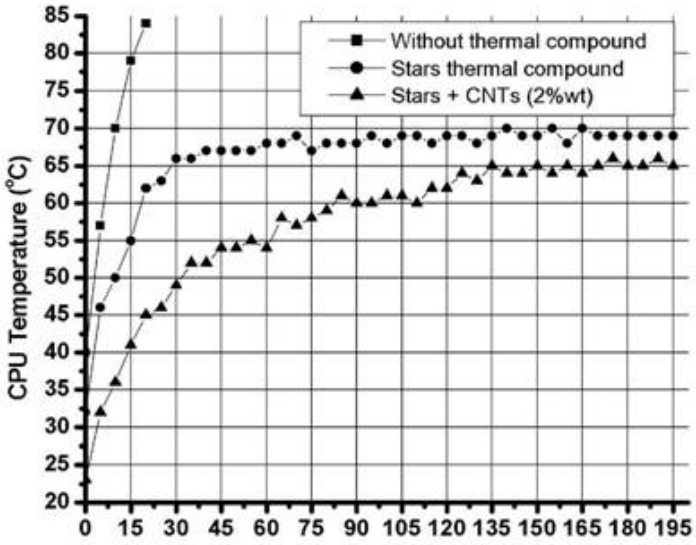

Figure 20: Difference in steady state temperature caused by mixing CNTs in silver paste compared to silver paste alone

The study on mixing randomly dispersed CNTs into a thermal compound discussed earlier used this type of comparative method to measure steady-state CPU temperature on varied samples under controlled heat input and airflow, the results of which are shown in Figure 20.

The level regions of the temperature vs. time curves denote the steady state

temperatures. The CPU temperature vs. time curves for the thermal compound with and without CNTs show that the addition of CNTs lowered steady state temperature. This comparative analysis justifies the conclusion that mixing in CNTs increased the heat sinks performance versus the thermal compound alone (Thang 2009). An expanded version of this deductive logic will be incorporated into the comparative testing method for our project, to examine the effects of aligned MWCNT arrays on convective heat transfer using the design, manufacturing, imaging, optimization, and testing techniques described in this section

Methodology

Sample Preparation

CNT Growth

Before template assisted CVD growth, our AAO templates needed to be cut into 4 mm x 7 mm samples, in order to completely cover the strain gage's heating element. Consistency was a focus, and only the most accurate samples were selected to ensure comparable testing. AAO templates were cut into 7 mm wide strips using a scalpel and the clamping setup shown in Figure 21. This 7 mm strip was then cut again every 4 mm into as many samples as possible.

Figure 21: Scalpel and clamping system used for cutting samples

Samples were loaded into a ceramic boat, which was then inserted into a one inch diameter quartz tube furnace and centered, shown in Figure 22. Next, the ends of the tube were connected to a controlled gas flow and vacuum system.

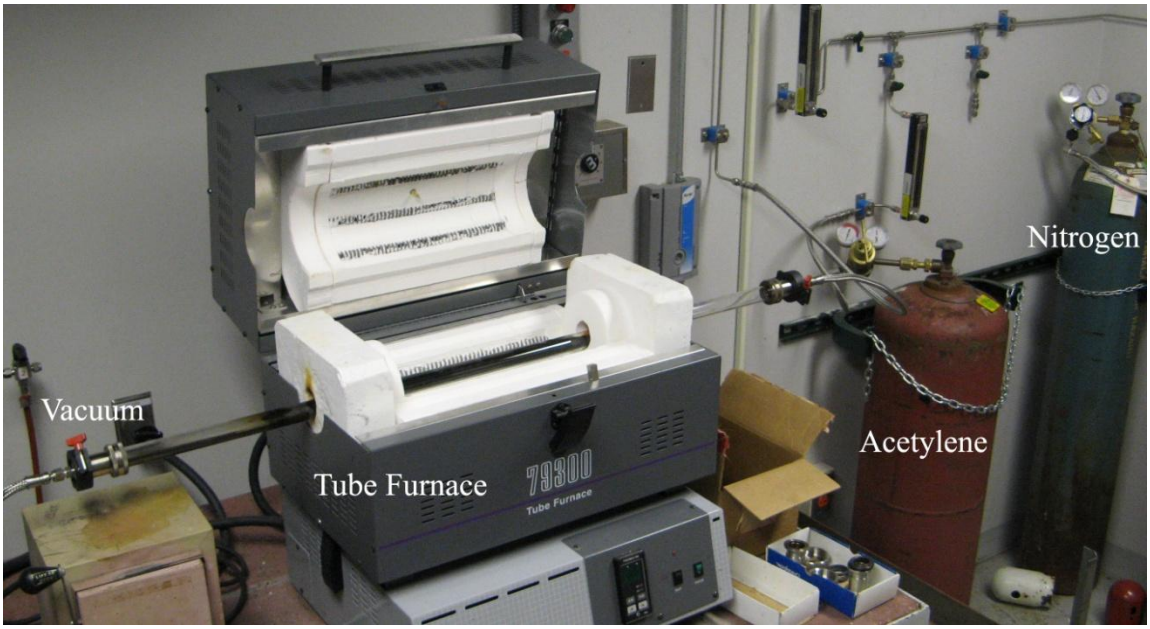

Figure 22: Tube furnace system used for chemical vapor deposition

Once the seal between the tube and the gas flow system was created, its integrity was tested using a procedure consisting of vacuum depressurization followed by pressurization by means of nitrogen gas flow into the tube. The tube was first closed off from the atmosphere, and then attached to a vacuum which was used to depressurize the tube to negative 0.5 bars. The system was subjected to this vacuum for one minute, then the vacuum was turned off, and the system was reopened to gradual nitrogen flow. The tube was then slowly re-pressurized with nitrogen at a flow rate of about 60 mm on our flow meter, until pressure within the tube exceeded atmospheric pressure, reaching 0.5 bars. The gas within the tube was then stabilized at this pressure for about a minute. This pressurization procedure was repeated three times from vacuum to 0.5 bars to ensure a good seal before beginning the chemical vapor deposition process with the tube at atmospheric pressure.

The furnace was set to increase at a rate of 10°C per minute up to 700°C, and gradual heating rate was used to avoid any effect of thermal shock on our samples. During heating, nitrogen flowed through the tube at a rate of 60 mm. Once at the desired temperature, a combined flow rate of nitrogen and acetylene was established by turning on the acetylene, and

adjusting the total flow rate to our desired concentration. A mix of 80% nitrogen and 20% acetylene was established using flow rates of 60 mm and 15 mm, respectively. This reaction occurred for one hour, and then the acetylene was turned off. The sample was left in the tube furnace to anneal at the set temperature for the next 12 hours. Once the annealing time was over, the furnace was turned off and allowed to cool gradually before removing the ceramic boat full of AAO templates, now with MWCNTs filling the nanopores and an annealed carbon layer on the surface. When the boat first comes out, the samples are buried by amorphous carbon. Some are concave up and some concave down coming out of the furnace as seen in Figure 23, which shows that this curvature is determined by the AAO template morphology, not the sample orientation when MWCNTs are grown. The samples had to be picked out using tweezers and separated from the junk carbon. Excess carbon was scraped off gently using a paper towel, resulting in clean samples ready for thermocleaning.

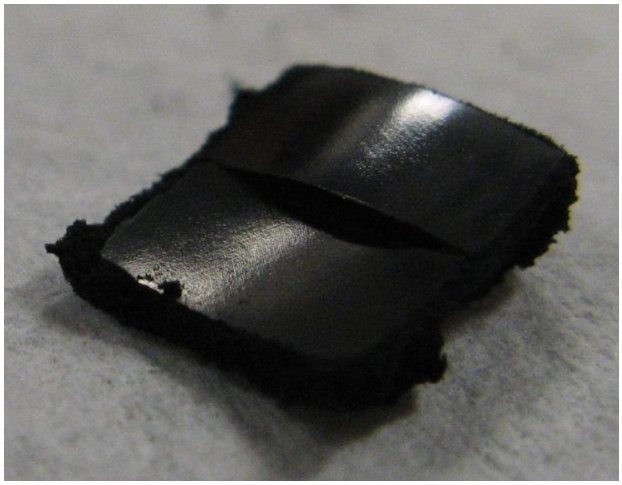

Figure 23: Samples after CVD with amorphous junk carbon on bottom

Thermocleaning Optimization

To optimize removal of the annealed carbon layer from the template surface, a parallel optimization process was used. Based on our prior knowledge of thermocleaning, we decided to investigate the effect of time at a temperature of 650ºC in the furnace pictured in Figure 24.

Samples were loaded into a ceramic boat as shown below in Figure 25, all concave down for consistency. Incremental thermocleaning times from 20 to 30 minutes were performed on samples, since we

Figure 24: Furnace used for thermocleaning

previously knew there is still annealed carbon on the surface at 20 minutes, and the MWCNTs themselves are burned off at 30 minutes.

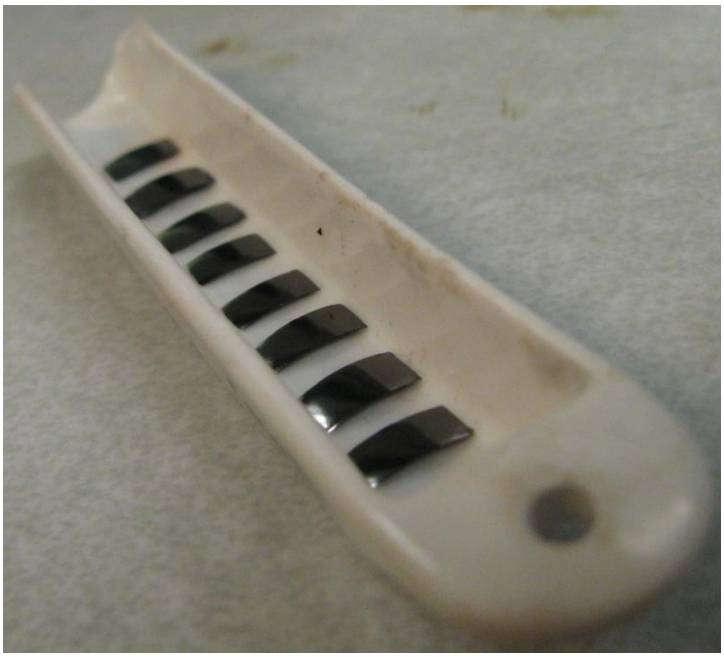

Figure 25: Samples loaded in ceramic boat for thermocleaning

Our first trial of thermocleaning resulted in total carbon burnout at 22 minutes, but we realized that the furnace's insulation was actually withholding substantial heat between trials. To address this, an hour was allowed for the furnace to cool down between concurrent thermocleaning trials. After resolving this process issue, we were able to obtain very good SEM images which provided us with an optimal thermocleaning time which fully removed the annealed carbon layer while leaving the MWCNTs intact. Top views of the sample surface morphologies for the incremental times were used for comparison.

The optimal morphology was seen at 28 minutes of thermocleaning, shown below in Figure 26. The whitest regions in the image represent the peaks of the AAO template, uncovered from the carbon layer. The MWCNTs can clearly be seen inside the pores.

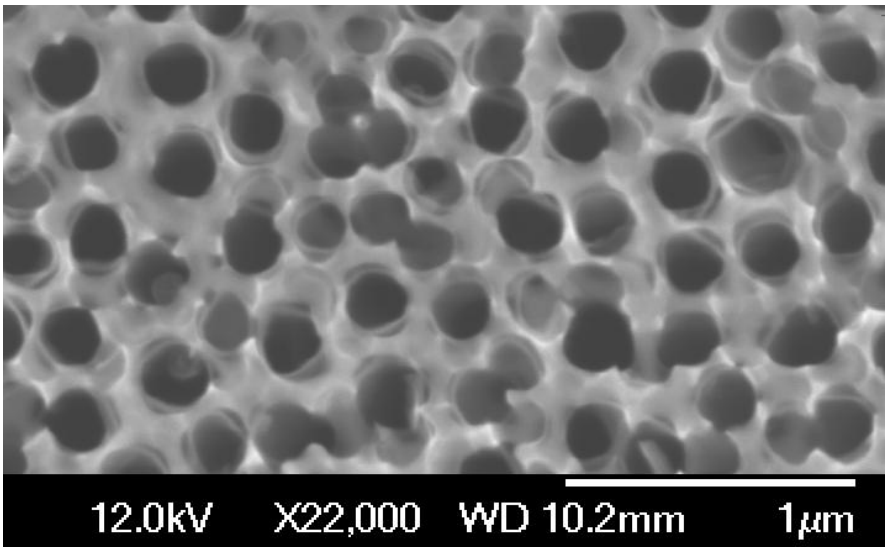

Figure 26: SEM image after 28 minutes of thermocleaning, showing exposed MWCNTs inside the nanopores

With a thermocleaning time established, an etching optimization procedure was performed, as described below.

Etching Optimization

The amount of ceramic template dissolved from the top and bottom of the sample is a function of time and acid concentration. A 0.5 Molar H_3PO_4 solution was chosen as the solvent for etching the Al_2O_3 based on previous experimental work done within our facilities. Using the same concentration, incremental times were tested in parallel.

Each etching consisted of submerging the sample into our solution using a concave etching platform elevated in a beaker with 500mL of solution Figure 27. The concavity of the platform lets the solution come in contact with both the top and bottom surface of the sample. For the first trial of our optimization, etching times were chosen to cover a wide range, from a hardly etched short pillar sample up to a substantially etched, long pillar sample. 10 min., 25 min., 1 hr., 2 hr., and 4 hr. intervals were chosen.

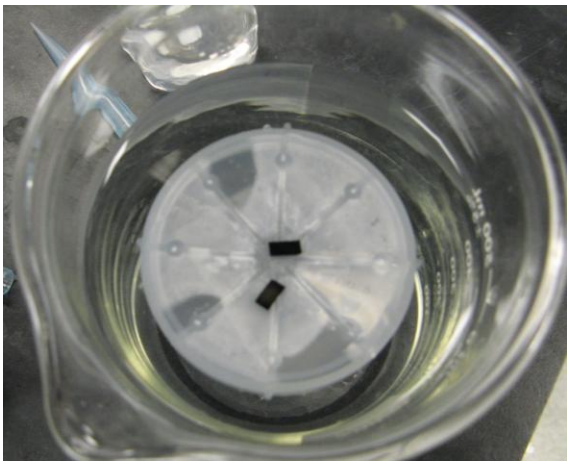

Figure 27: Samples being acid etched on a concave surface

After the respective time, the sample was removed with tweezers and thoroughly rinsed with distilled water. After drying, the samples were inspected using SEM. Results are shown below in Figure 28. A comparison between the 25 minute and 4 hour sample is shown, both showing slightly exposed MWCTs. Each sample was broken into tiny pieces, and there were clear differences between different areas of the same sample. Observations of surface morphology showed variation between different sections of the rectangles; perhaps the outside edges were more etched.

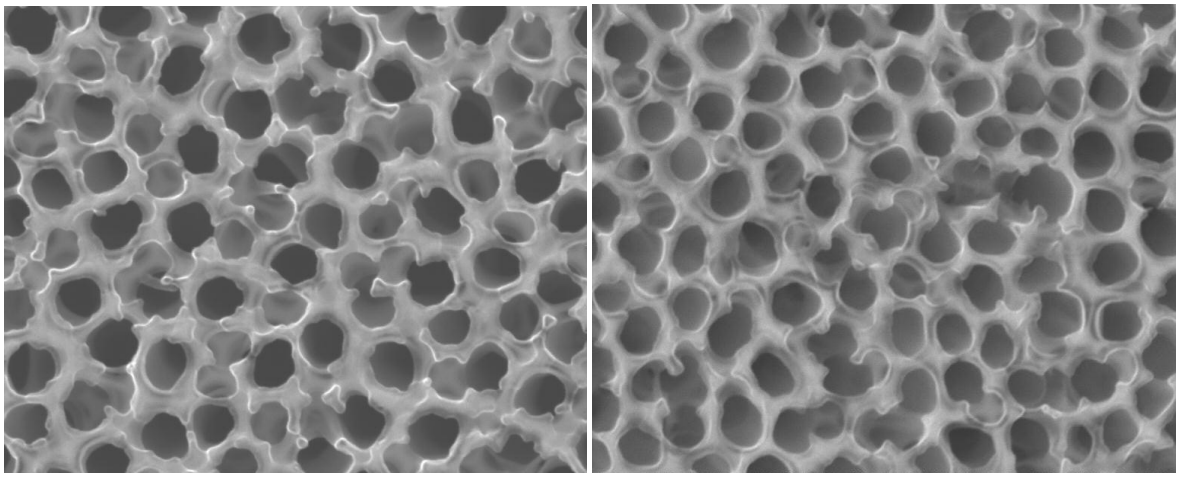

Figure 28: left: 25 minute etch, right: 4 hour etch

Comparative Testing

Testing Setup

For our testing setup, samples were stacked on top of a strain gage heater, with a thin layer of silicon based thermal grease as the thermal interface material. To monitor the internal temperature over time ($T_{internal}$ vs. time), a glass micro-bead thermistor (Figure 29), was mounted underneath the heater. This tiny glass encapsulated piece of semiconductor varies in resistance as temperature changes, and can be calibrated to give accurate temperature readings.

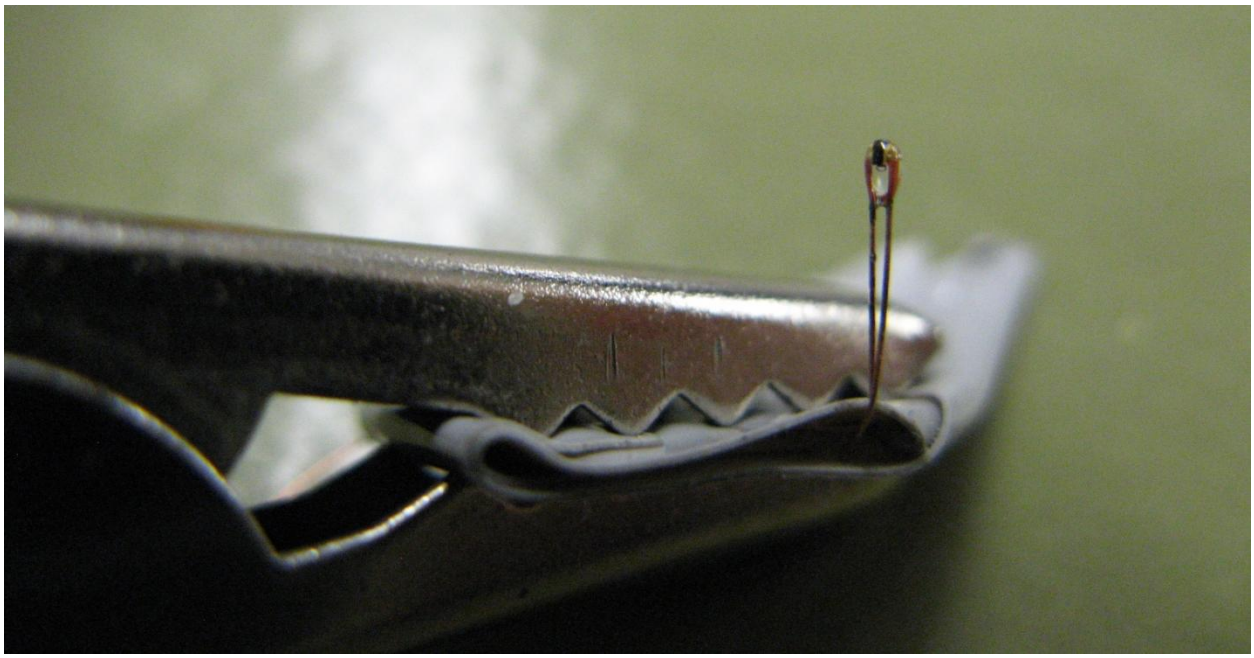

Figure 29: Micro-bead thermistor

Figure 30 below shows a schematic of our experimental setup.

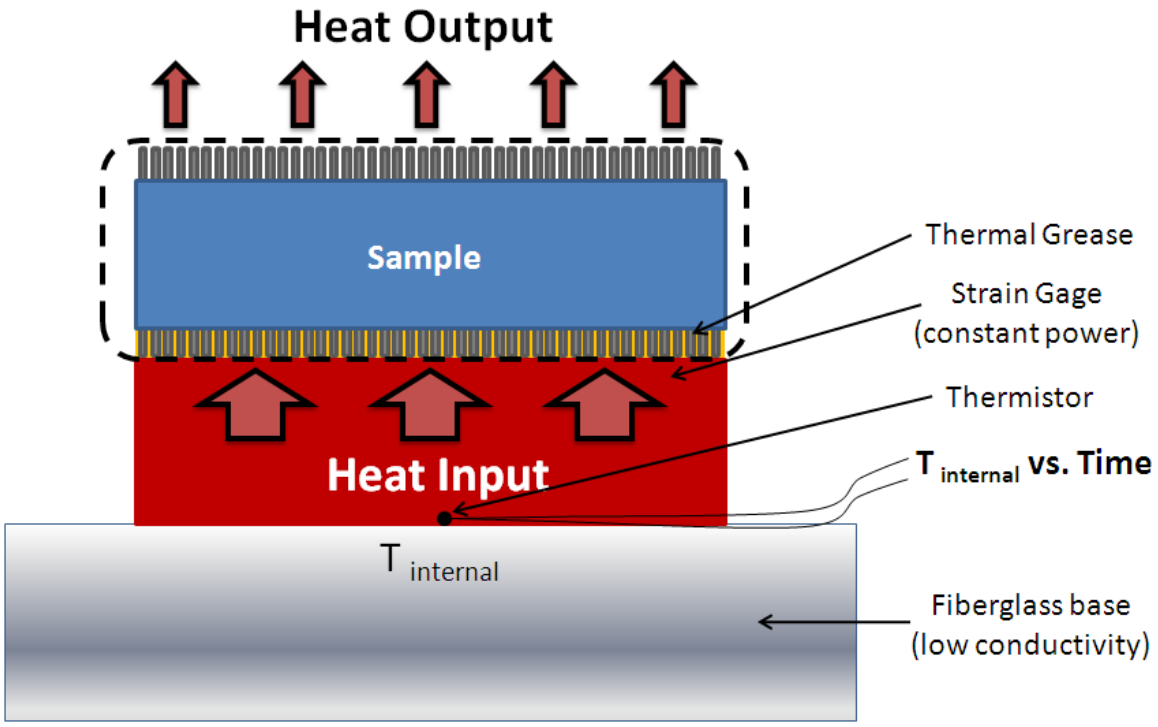

Figure 30: Schematic showing stacking of experimental setup

To quantify the change in convective properties between samples, each sample (blue) is provided constant heat input using a strain gage (red) powered by a constant voltage. The approximate thermodynamic system is designated by the dotted line, and the red arrows for heat input and output. The whole setup is mounted on a fiberglass base with an extremely low thermal conductivity of 0.58 W/mK to minimize external heat loss (K-Mac 2009). The physical setup is shown in Figure 31 below. The thermistor is inset into the fiberglass base by drilling a small hole, allowing the heater to lie flat on top.

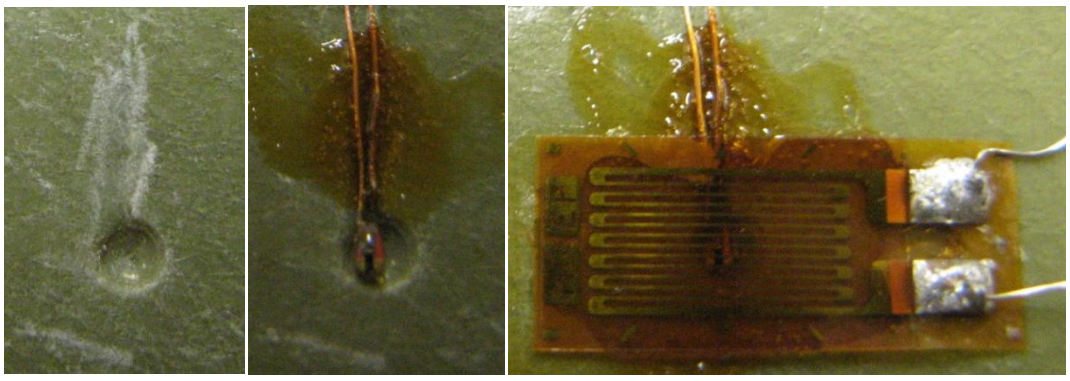

Figure 31: Physical stacking of strain gage on top of thermistor, showing the drilled hole and thermal grease

To measure temperature using our thermistor, a circuit was built to measure the resistance over time, which was then calibrated to determine temperature at a given resistance value. An excitation voltage was applied to a voltage divider circuit, with the thermistor in series with a known resistance value (120 Ω) strain gage, shown below in Figure 32. The excitation voltage and the voltage across our known resistor were monitored over time using a virtual instrumentation program, discussed later in this section. With this information, our program calculated the resistance of the thermistor every 0.25 seconds and recorded the data to a spreadsheet.

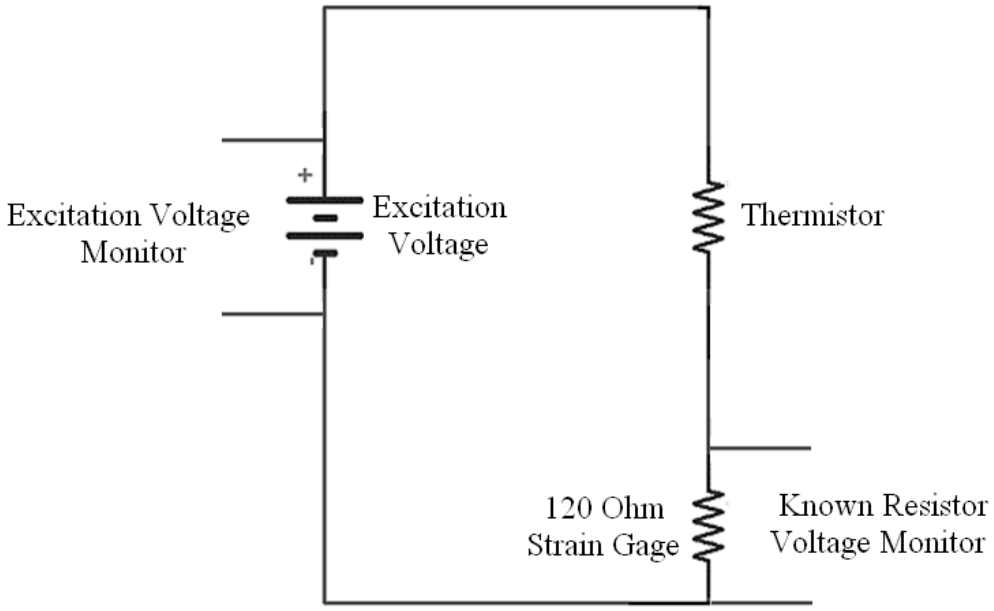

Figure 33: Schematic of the voltage divider circuit used in our experiment

The physical circuit is shown below ready for testing, with a sample mounted and the alligator clips connected (Figure 33).

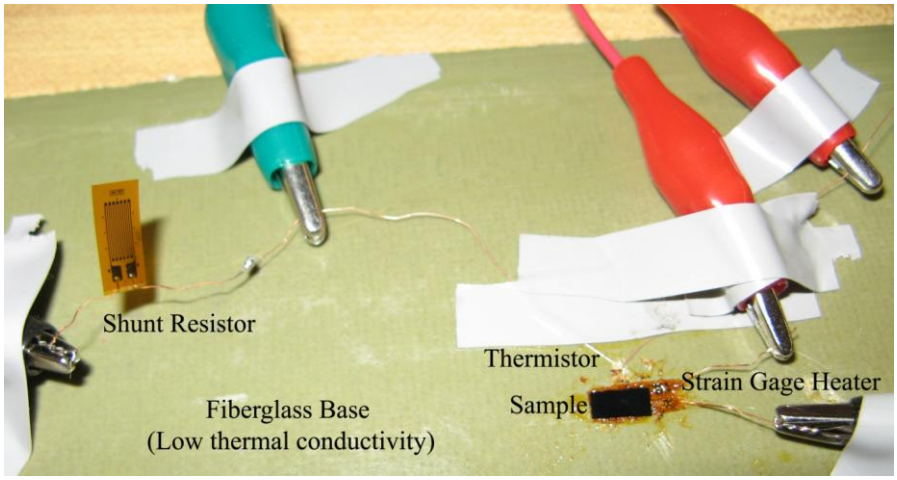

Figure 32: Physical circuit with alligator clips supplying voltage and monitoring resistance

This whole setup was covered with a plastic bin during the tests (Figure 34), which greatly reduced airflow fluctuations within the room and maintained a steadier ambient temperature. The alligator clips which supply power to the strain gage heater were connected to the constant voltage source. The rest of the clips connected to our Data Acquisition device (DAQ), which supplied an excitation voltage to the thermistor circuit, monitored that voltage, and monitored the voltage across the known resistor.

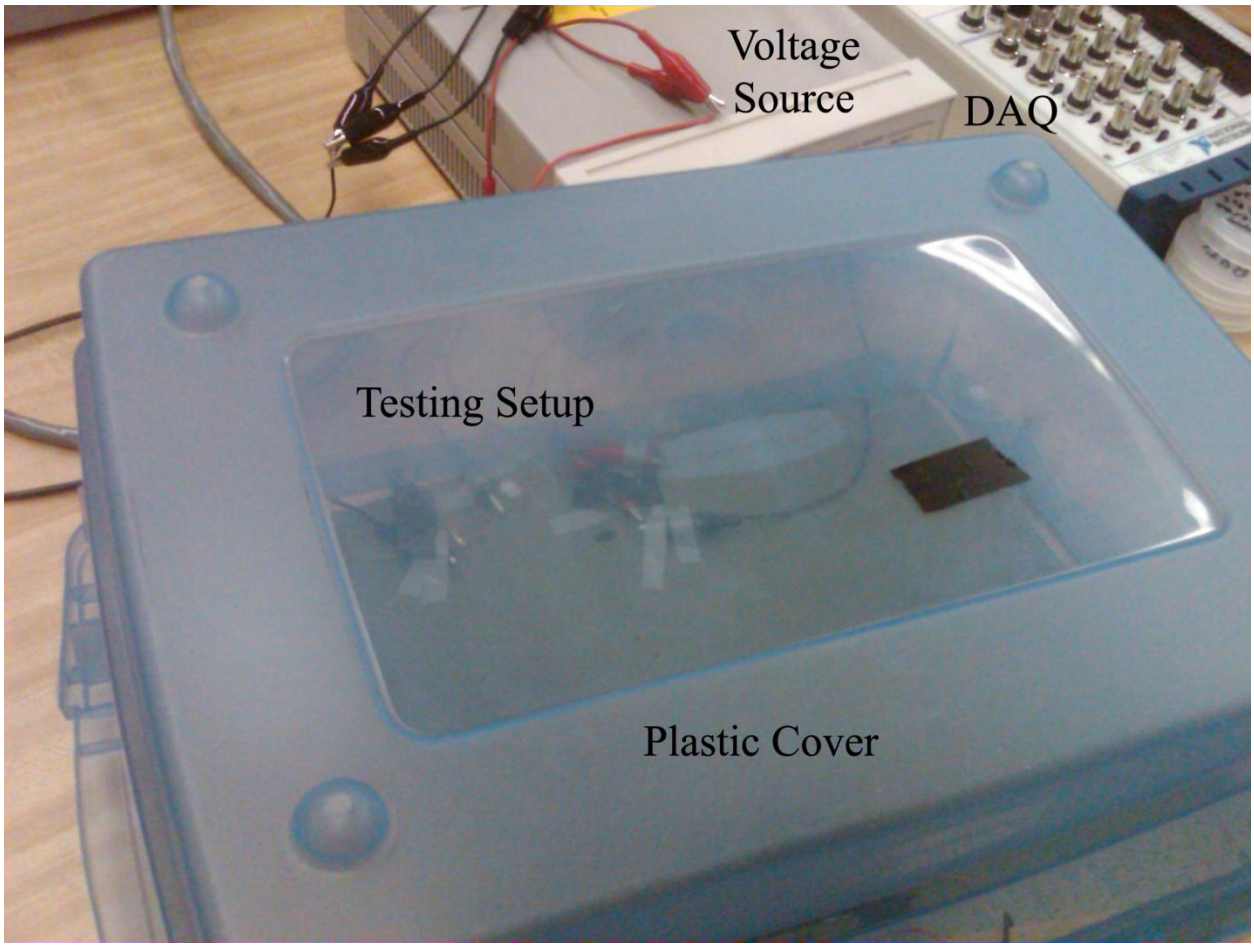

Figure 34: Testing setup covered by plastic bin to limit air fluctuations

Virtual Instrumentation

To perform the thermal testing necessary for our investigation, we first needed an effective method to monitor the temperature over time via our thermistor. A virtual instrument (VI) was created in National Instruments LabView for this purpose; the block diagram programming logic is shown in Figure 35.

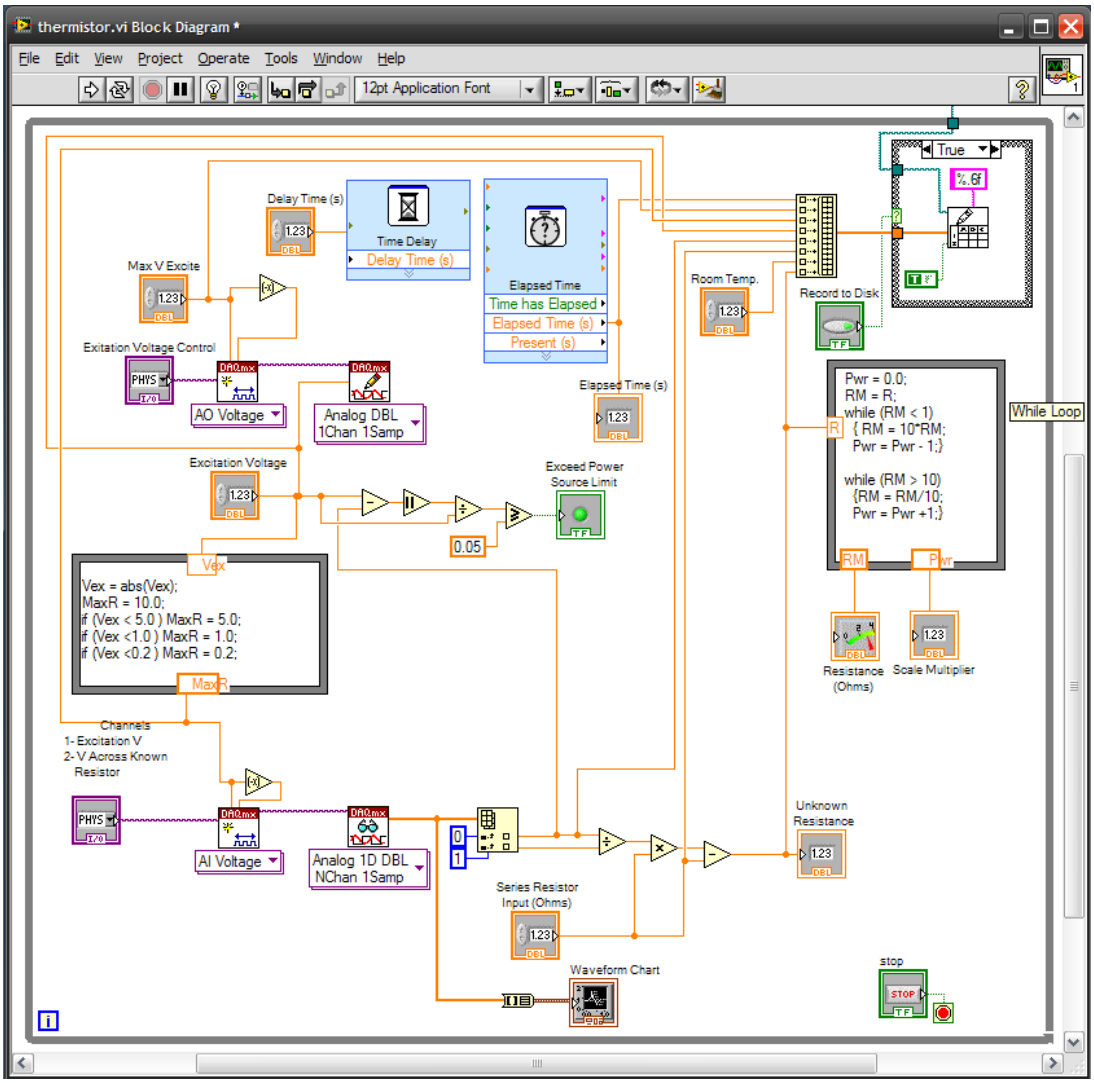

Figure 35: Block diagram showing the programming logic of our virtual instrument

Figure 36 below shows the equation used within our VI program to calculate the resistance of the thermistor (R1) with respect to the excitation voltage (V_{in}) and the voltage across the known 120Ω strain gage R2 (V_{out}).

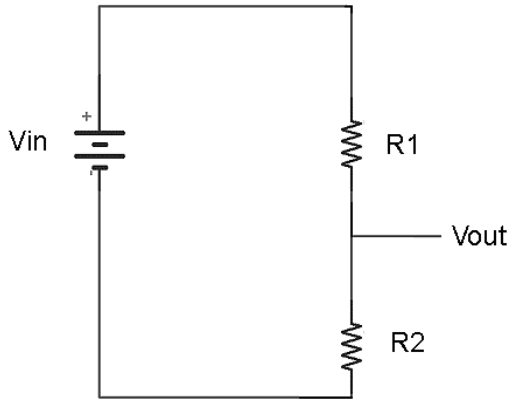

$$Vout = Vin \times \frac{R2}{R1+R2}$$

Figure 36: Voltage divider schematic and equation

From this equation, R1 = (R2*V_{in} / V_{out}) – R2. The section of our VI responsible for this calculation is shown in Figure 37. V_{in} is channel 0, and V_{out} is channel 1, as denoted by the blue boxed numbers. The division, multiplication, and subtraction boxes are the logic which executes this formula to calculate R2, the thermistor resistance value.

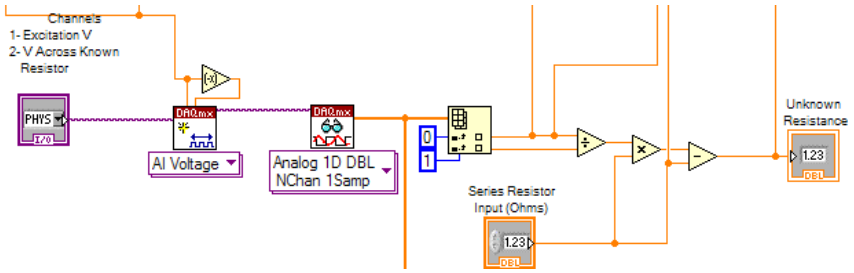

Figure 37: Section of programming logic that performs the voltage divider equation

The section of our programming logic shown below in Figure 38 enables our VI to read resistance accurately at the large range of resistance values that are encountered in heating the system. When the resistance of the thermistor is high, the voltage across the known resistor is low, and vice versa for when the thermistor has a low resistance at hot temperatures. The program accounts for this by adjusting the excitation voltage according to the thermistor resistance.

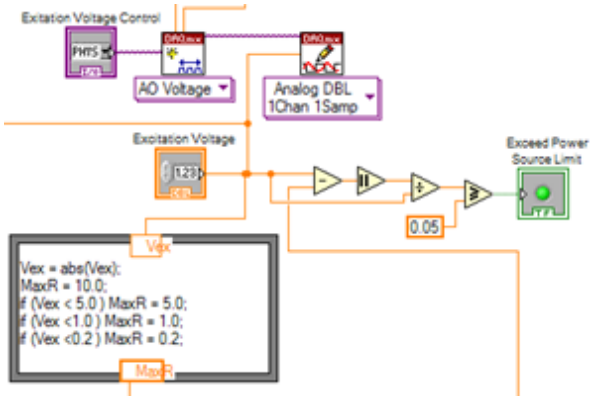

Figure 38: Section of programming logic which adjusts the excitation voltage to account for high resistances

The block diagram results in the front panel shown in Figure 39. The analog output and input boxes set the channels used by the DAQ, and the maximum acceptable excitation voltage and known resistor values are controlled. The resistance information box displays the thermistor resistance in real time as the experiment is performed, and converts the values into scientific notation. The room temperature of each trial is also input in this box. The elapsed time and the file path are shown in the bottom left corner.

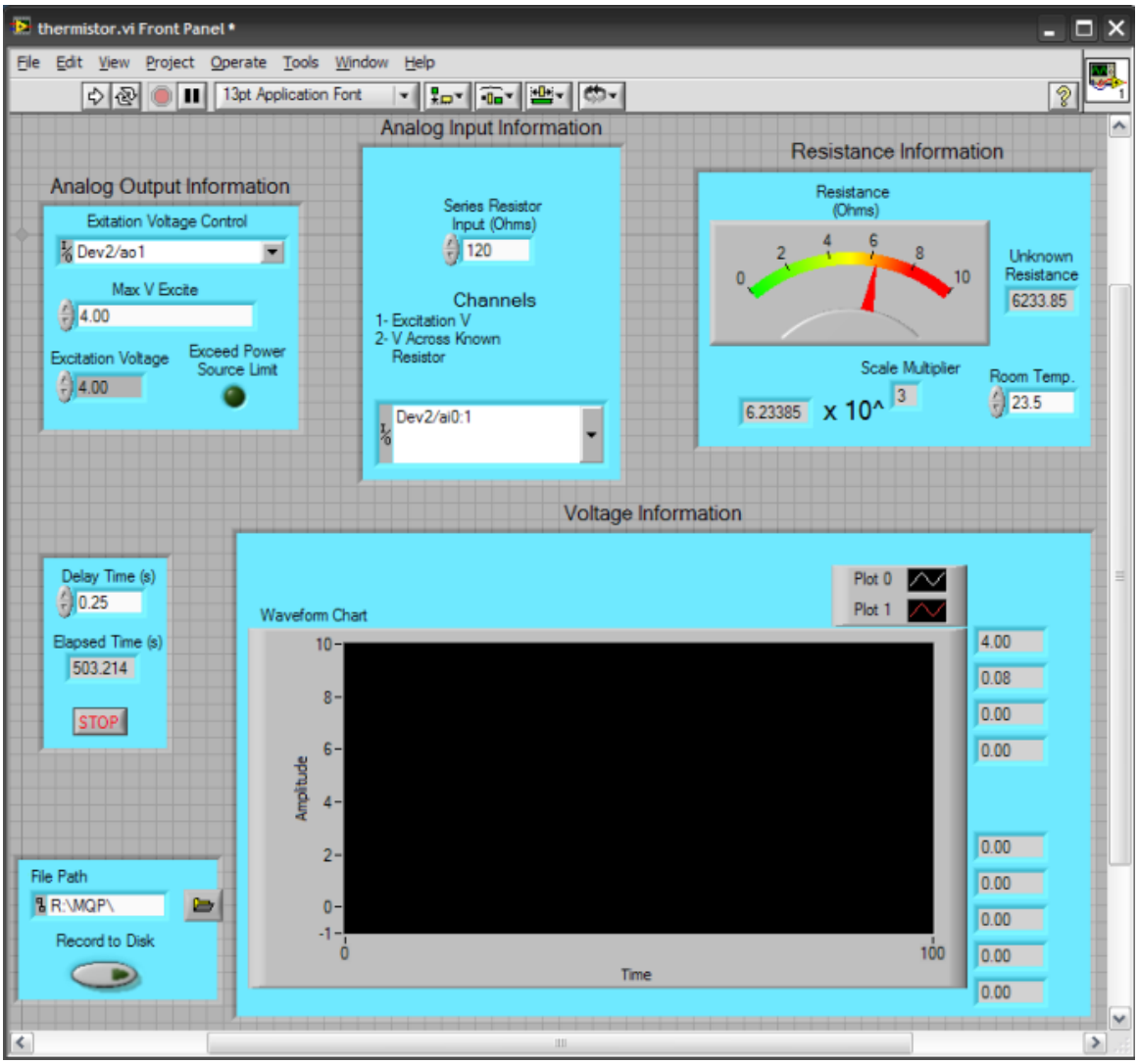

Figure 39: Front panel of our virtual instrument

Thermal Testing Technique

Thermal testing was performed on many occasions for the different morphologies that exist at each step in our sample preparation, and a blank heater with no sample on top as the control. When the heater is activated, the $T_{internal}$ increases from room temperature up to a steady state temperature, where the heat input approximately equals the heat output. When the heater is turned off, the system will eventually reach room temperature again. The $T_{internal}$ vs. time data for this process was collected for each sample, and steady state temperatures were compared. A sample with better convective surface properties should have a lower steady state temperature.

To enable comparative analysis for our testing method, data was gathered for the AAO template alone, the template with MWCNTs grown before thermocleaning (annealed carbon surface layer), after thermocleaning (unexposed MWCNTs), and for thermocleaned then etched. Between each trial, the entire setup was given a full hour to cool back down to room temperature. Each sample trial included a 60 second run at room temperature, then another run where the heater was activated after ten seconds of recording, and the data was recorded for about 500 seconds.

Temperature Calibration

To convert the resistance curves to temperatures, a calibration procedure needed to be performed. The thermistor was connected to the same circuit as usual, and resistance curves were recorded, along with a thermometer reading, at temperatures from 0°C in an ice water bath up to 90°C in nearly boiling water. The hot water was cooled gradually using ice, and at about ten degree intervals, a resistance curve was recorded.

An average resistance was determined for each temperature, and the resistance vs. temperature data was plotted in Excel. Our calibration data is shown below in Figure 40. A best-fit exponential curve equation was obtained to describe the data points we collected, shown to the right of the graph.

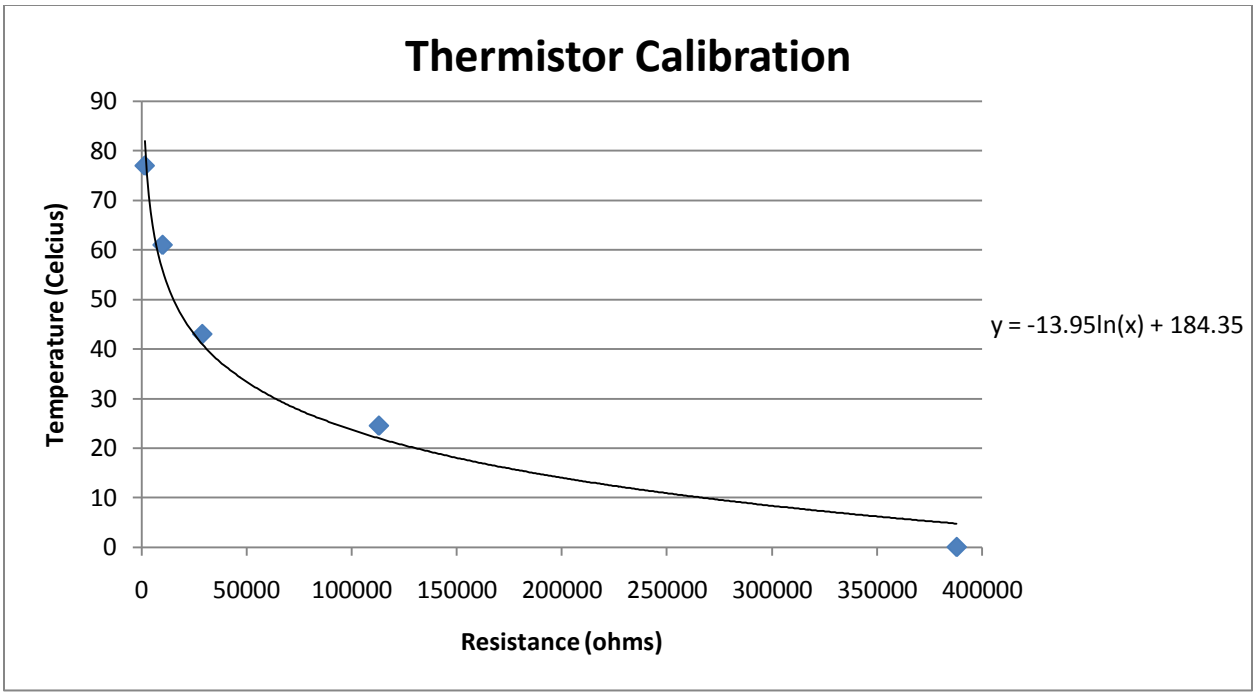

Figure 40: Thermistor calibration graph with best fit equation

With this equation, resistance data can be converted to temperature by plugging the resistance value as x. An example of a data set before and after converting to temperature is shown in Figure 41.

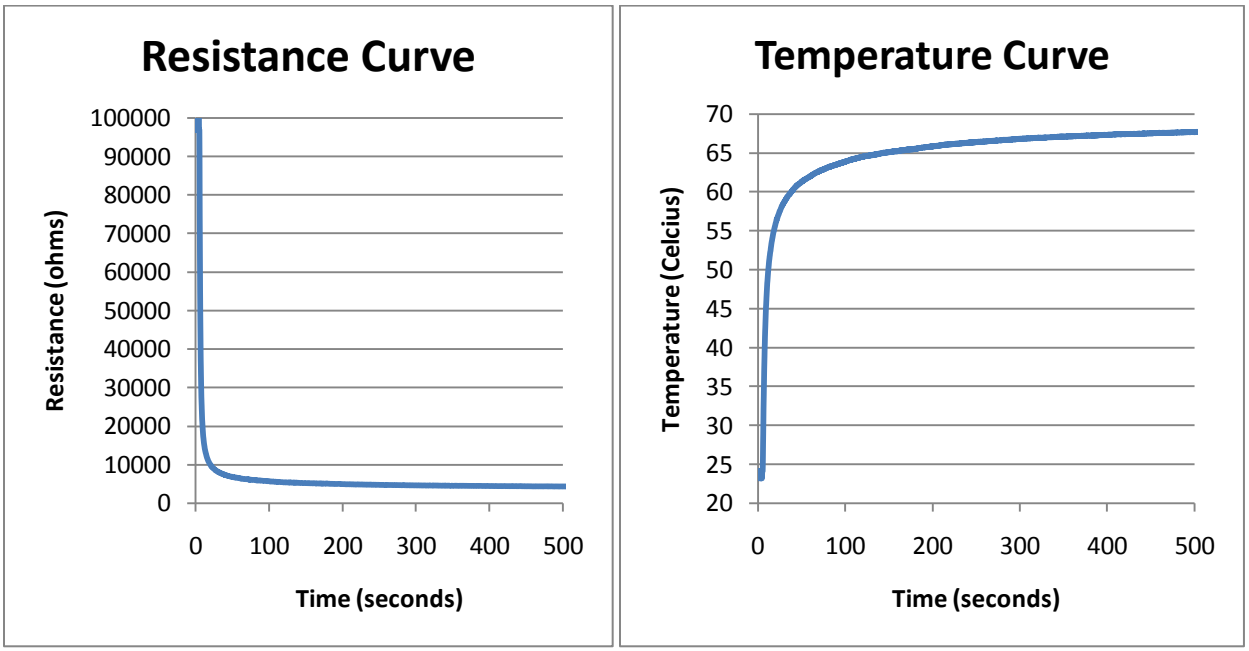

Figure 41: Resistance to temperature conversion after calibration

Results and Analysis

Over 12 days of testing, we produced a quantity of results to be processed and analyzed. Our first objective was to ensure that our testing method was repeatable, and that the results from different morphologies were distinguishable. For clarity, Table 1 below designates the abbreviations that will be used for the different samples.

Sample Morphology	Abbreviation
Heater alone	Blank
AAO template alone	Temp
Template with MWCNTs grown	Unthermo
Template with MWCNTs grown, and thermocleaned	Thermo
Template with MWCNTs grown, thermocleaned, and etched	Etched

Table 1: Morphologies tested with abbreviations

Figure 42 below shows two trials of the temperature vs. time curves obtained for the heater alone, and an unthermocleaned sample. Testing was alternated from blank to unthermo, with 6.5 Volts applied to the strain gage heater. The same setup was used for both trials.

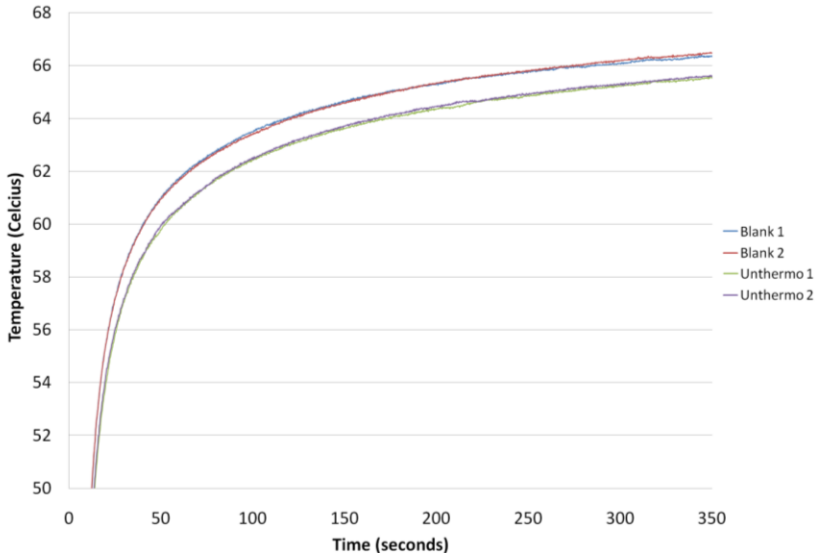

Figure 42: Consistency between multiple trials of the same samples

This graph shows consistency between trials with the same morphology, and a clear difference between the heater alone and with a sample on top. The steady state temperature of the unthermocleaned sample is about one degree Celsius lower than that of the blank heater. This shows that heat is moving more easily through the sample than from the heater to air alone, therefore working as a heat sink. The curves never truly reach a constant steady state temperature, since some heat is transferred and stored in the fiberglass base, which has an extremely low, but not negligible thermal conductivity.

Three examples of the cool-down section of the curve are shown below in Figure 43, but they are virtually indistinguishable due to the data acquisition device's bit size capabilities, so this portion of the curve was not recorded in consequent trials.

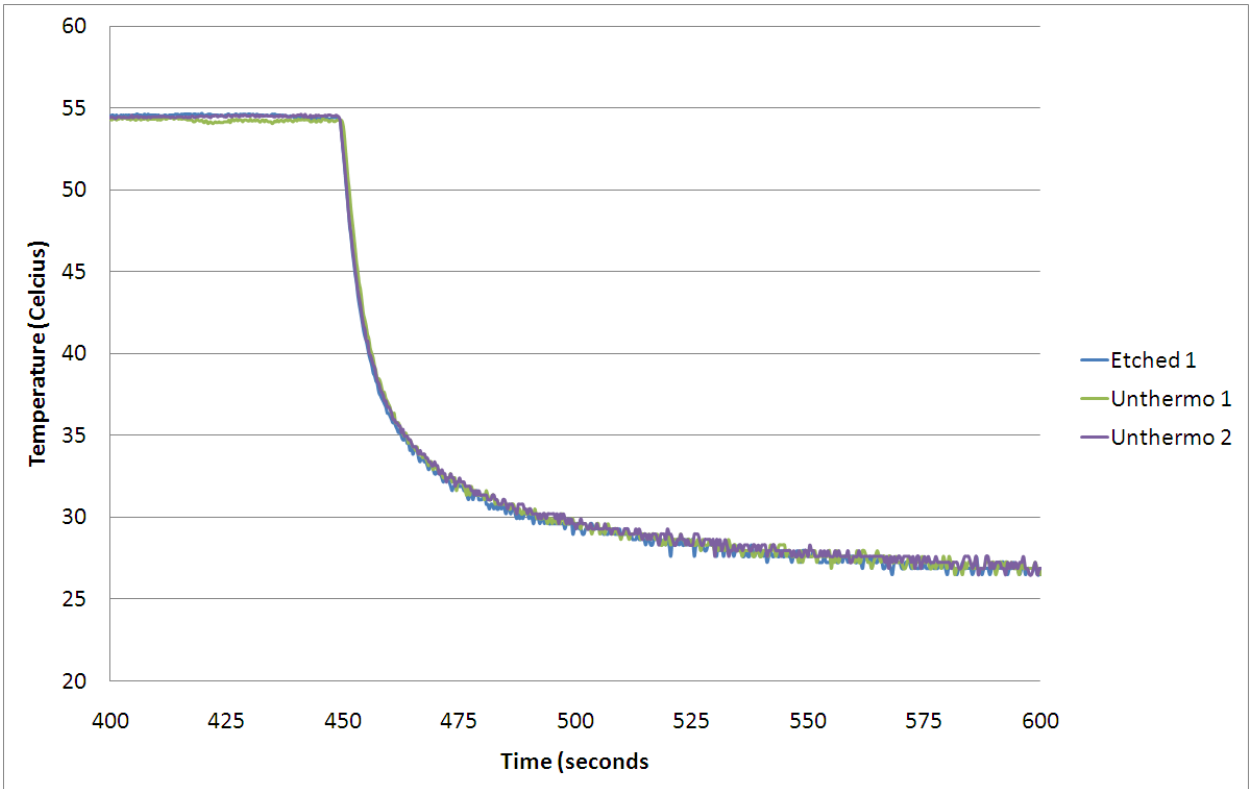

Figure 43: Cool down curves after heater is turned off

The next graph (Figure 44) shows a blank heater, an empty template, and two different etched samples. At a higher voltage of 7.5 V, the steady state temperature differences between

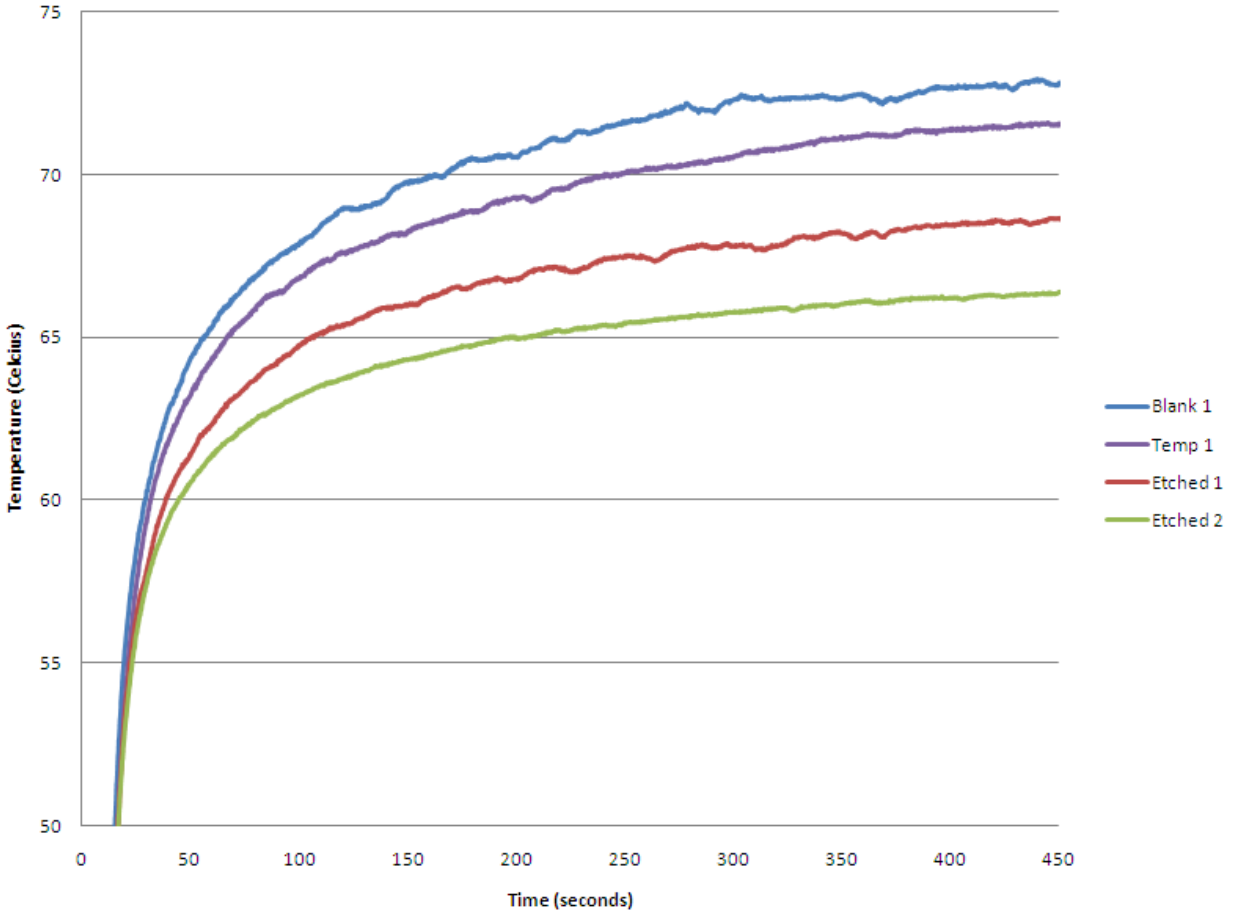

Figure 44: Temperature vs. time curves for blank, template, and two different etched samples

samples are more obvious, due to the exponential curve used to calibrate to temperature. Both etched samples have lower steady state temperatures than the template, but they show significant differences with each other. The slope of the steady state portion of the curve is approximately equal between the etched samples, both lower compared with the slopes seen in the template and the blank curves. It appears that the etched samples outperformed the template in terms of heat transfer efficiency to the surrounding air, but the difference between the two etched samples could be due to the sample mounting (thermal grease layer thickness, possible air pockets, or thermal contact area with heater), or the length of exposed CNT tips.

Relative performance differences were seen between similar samples throughout all the trials, but there are relevant consistencies within the entire data set, and the inconsistencies seen

could be due to a variety of uncontrollable factors. Figure 45 below shows three complete sets of comparative morphology data.

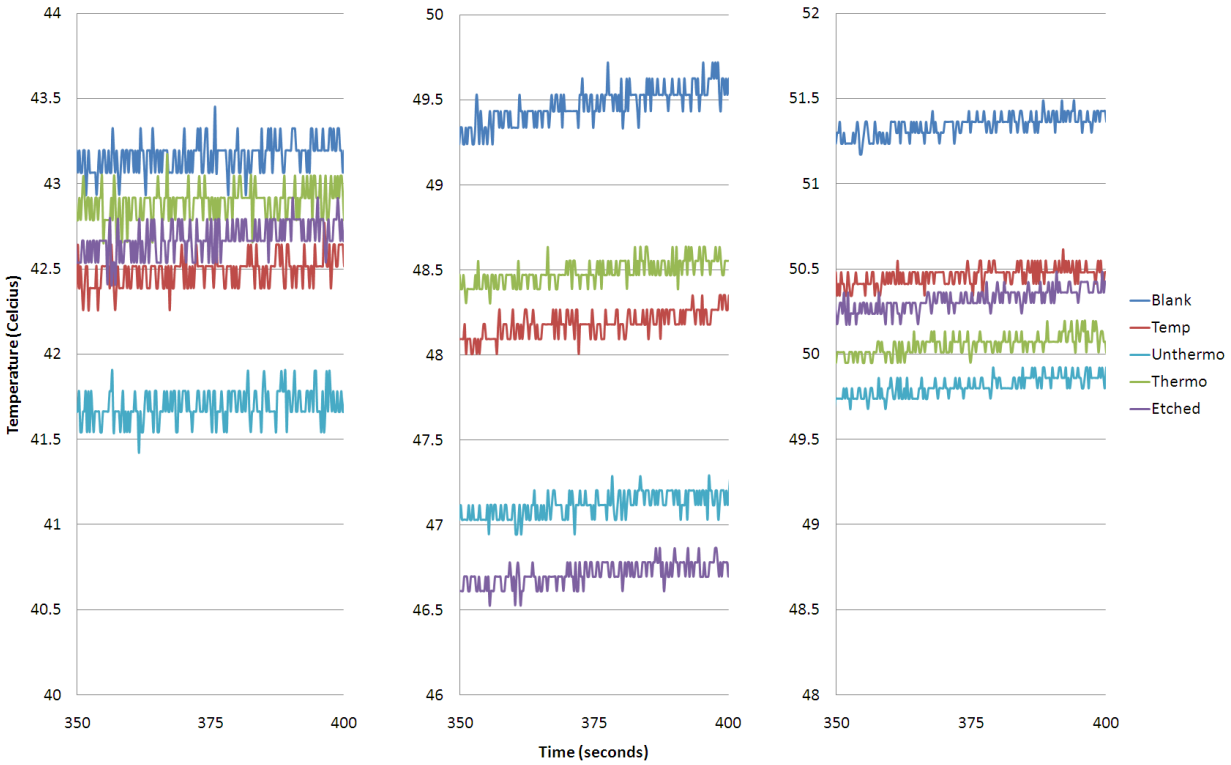

Figure 45: Comparative analysis of all tested morphologies for three separate trials

The relative positions of the blank heater (dark blue), empty template (red), and unthermocleaned (light blue) are the same in each of the trials. These are the most consistent samples since there is no additional processing after CNT growth. The thermocleaned and etched samples vary in their relative position between trials, likely caused by subtle differences in their processing parameters. In the left (4.5 V), thermo and etched did not perform as well as the empty templates, possibly indicative of excess thermocleaning time. For the center and right trials (5.5 V), the thermocleaning time was reduced from 28 to 27.5 minutes. The etched sample was the most effective in the center trial, but this behavior was not seen elsewhere in our testing. This could be due to minor morphology differences or inconsistent thermal connections between sample and heater. In the right trial, thermo and etched both fell between the template and the unthermo sample, with thermo lower than etched. Again, this could be due to sample mounting differences, or perhaps combustion of the CNTs due to excess thermocleaning.

The next graph (Figure 46) shows the same blank, and unthermo pattern seen in the trials above, but this time compared with copper foil mounted on the heater using thermal grease. The copper clearly outperforms any of the AAO template based samples, as would be expected due to its extremely high thermal conductivity.

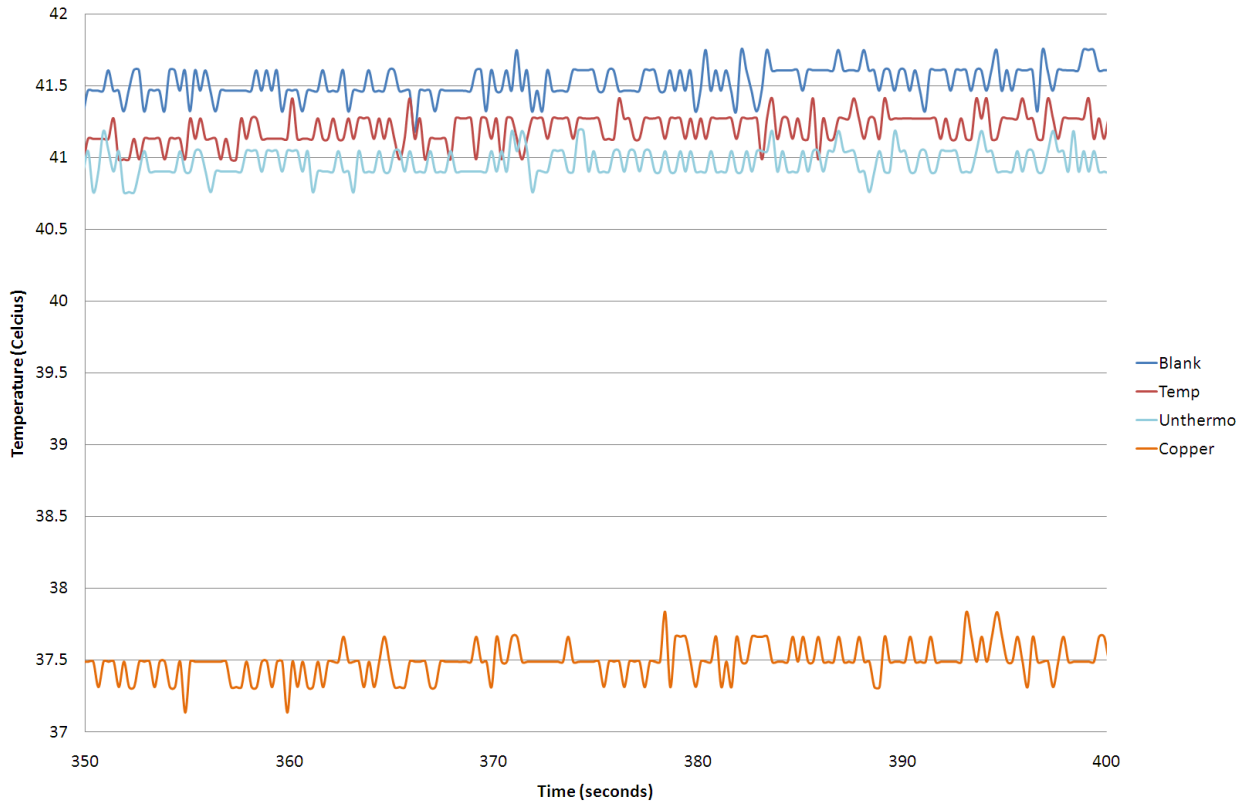

Figure 46: Steady state temperatures of blank, temp, and unthermo compared with bulk copper

Our results demonstrate that our testing method is both consistent and effective. Comparative analysis between sample morphologies was possible, and valuable information was obtained from our data. We showed that the blank heater, empty template, and unthermocleaned samples performed consistently with respect to one another, and that the processed samples (thermocleaned and etched) were different between trials. This is to be expected since processing parameters can have variations which affect the critical traits of individual samples.

Conclusions

After performing our experiments, we were able to obtain some clear results and conclusions about the heat transfer properties of our nano-structured surfaces to the ambient air. Even though the AAO templates have a known thermal conductivity of 40 W/mK, growing MWCNTs which have a lower thermal conductivity of 10 W/mK, still enhanced heat transfer. Our results suggest that there are definitely some unique heat transfer properties due to the nano-scale three-dimensional annealed carbon layer. The processed samples were less predictable, since minor differences in processing parameters can cause variations which affect the performance of individual samples. These inconsistencies are difficult to avoid, since the variations in processing are sometimes out of the range which we can accurately control. Unthermocleaned samples were shown to consistently have the best convective heat transfer properties.

Future research could potentially narrow down the uncertainty we observed, and the processing parameters have potential to be further optimized for better results. Also, there are many other CNT morphologies that could be used effectively for this type of micro and nano scale heat transfer. Different manufacturing techniques altogether or further improvements of our native processes could be a part of improving these results. As electronics continue their trend of miniaturization, investigation of nano scale convection properties are sure to continue. We are happy to help open this window for future progress, and look forward to continued research in the area.

Bibliography

Belwalkar, A., E. Grasing, W. Van Geertruyden, Z. Huang, and W. Z. Misiolek. "Effect of Processing Parameters on Pore Structure and Thickness of Anodic Aluminum Oxide (AAO) Tubular Membranes." *Journal of Membrane Science* 2nd ser. 319.1 (2008): 192-98. Print.

"Carbon, its Allotropes and Structures." *EveryScience*. Web. 11 Dec. 2009. <http://www.everyscience.com/Chemistry/Inorganic/Carbon/a.1189.php>.

Conway, Paul, David Whalley, and Farhad Sarvar. "Thermal Interface Materials - A Review of the State of the Art." *Electronics Systemintegration Technology Conference* (2006): 1292-302.

Demczyk, B. G., Y. M. Wang, J. Cumings, M. Hetman, W. Han, A. Zettl, and R. O. Ritchie. "Direct Mechanical Measurement of the Tensile Strength and Elastic Modulus of Multiwalled Carbon Nanotubes." *Materials Science and Engineering* A334 (2002): 173-78.

"Fiberglass Sheets and Plates by K-mac Plastics." *Plastic Sheets, Rods and Tubes by K-mac*. Web. 07 Dec. 2009. <http://k-mac-plastics.com/fiberglass-sheet.htm#VO>.

Garimella, Suresh. "Advances in mesoscale thermal management technologies for microelectronics." *Microelectronics Journal* 37 (2006): 1165-185. Print.

Goldstein, G. I., D. E. Newbury, P. Echlin, D. C. Joy, C. Fiori, and E. Lifshin. *Scanning Electron Microscopy and X-Ray Microanalysis a Text for Biologists, Materials Scientists, and Geologists*. New York: Plenum, 1981.

Hong, Seunghun, and S. Myung. "Nanotube Electronics: A Flexible Approach to Mobility." *Nature Nanotechnology* 2.4 (2007): 207-08.

Hu, Guofeng, Haiming Zhang, Wenwen Di, and Tingting Zhao. "Study on Wet Etching of AAO Template." *Applied Physics Research* 1.2 (2009): 78-82. Print.

Jimenez, Guillermo A., and Sadhan C. Jana. "Electrically Conductive Polymer Nanocomposites of Polymethylmethacrylate and Carbon Nanofibers Prepared by Chaotic Mixing." *Composites: Part A* 38 (2007): 983-93. Print.

Kim, P., L. Shi, A. Majumdar, and P. L. McEuen. "Thermal Transport Measurements of Individual Multiwalled Nanotubes." *Physical Reviews Letters* 87.21 (2001).

Klesel, Josh. "Scanning Electron Microscopy." *Materials Science and Engineering*. Iowa State University. Web. 25 Nov. 2009. <http://mse.iastate.edu/microscopy/home.html>.

Kordas, K., G. Toth, P. Moilanen, M. Kumpumaki, J. Vahakangas, A. Uusimaki, R. Vajtai, and P.M. Ajayan. "Chip cooling with integrated carbon nanotube microfin architectures." *Applied Physics Letters* 90.123105 (2007). Print.

Li, C. Papadopoulos, J. M. Xu, and M. Moskovits, Appl. Phys. Lett. 75, 367 s1999d.

Li, Jun, and Meyya Meyyappan. Nanoengineered Thermal Materials Based on Carbon Nanotube Array Composites. The United States of America as Represented by the Administrator of the National Aeronautics and Space Administration, assignee. Patent 7,273,095 B2. 25 Sept. 2007.

Lu, Shijing, Zixue Su, Jian Sha, and Wuzong Zhou. "Ionic nano-convection in anodization of aluminum plate." *ChemComm* (2009): 5639-641. Print.

Melechko, A. V., V. I. Merkulov, T. E. McKnight, M. A. Guillorn, K. L. Klein, D. H. Lowndes, and M. L. Simpson. "Vertically Aligned Carbon Nanofibers and Related Structures: Controlled Synthesis and Directed Assembly." *Applied Physics Reviews* 97 (2005).

Naeemi, Azad, and James D. Meindl. "Carbon Nanotube Interconnects." Proc. of 2007 International Symposium on Physical Design, Austin, Texas, USA. Print.

"Nanotechnologies: Carbon nanotubes." *Rob Aid presents robots, gadgets. tech and bionics*. Web. 11 Dec. 2009. <http://www.robaid.com/tech/nanotechnologies-carbon-nanotubes.htm>.

Ngo, Quoc, Brett Cruden, Alan Cassell, Gerard Sims, M. Meyyappan, Jun Li, and Cary Yang. "Thermal Interface Properties of Cu-filled Vertically Aligned Carbon Nanofiber Arrays." *Nano Letters* 4.12 (2004): 2403-407. Print.

Page, M. "Intel Stock Core 2 Duo Radial Curved Bifurcated Fin Heatsink Review." *Frosty Tech*. 2009. Web. <http://www.frostytech.com/articleview.cfm?articleID=2132>.

Pradhan, N.R., H. Duan, J. Liang, and G.S. Iannacchione. "Specific heat and thermal conductivity measurements for anisotropic and random macroscopic composites of cobalt nanowires." *Nanotechnology* 19 (2008). Print.

Prasher, Ravi. "Thermal Interface Materials: Historical Perspective, Status, and Future Directions." *Proceedings of the Institute of Electronics and Electronics Engineers* 94.8 (2006): 1571-586. Print.

Shaikh, Shadab, Khalid Lafdi, and Edward Silverman. "The effect of a CNT interface on the thermal resistance of contacting surfaces." *Carbon* 45 (2007): 695-703. Print.

Son, Won Il, Joo-Hee Hong, and Jae-Min Hong. *Fabrication of micro-heat sink by nanotemplate synthesis and its cooling characteristics*. Rep. Cheongryang, Seoul, Korea:

Optoelectronic Materials Research Center, Korea Institute of Science and Technology, 2005. Print.

"Space Elevator Concept." *The LiftPort Space Elevator*. LiftPort Group. Web. 10 Dec. 2009. <http://www.liftport.com/>.

Thang, Bui Hung, Phan Ngoc Hong, Phon Hong Khoi, and Phon Ngac Minh. "Application of multiwall carbon nanotubes for thermal dissipation in a micro-processor." *Institute of Physics Electronic Journals*. 2009. Web.

Thostenson, Erik T., Zhifeng Ren, and Tsu-Wei Chou. "Advances in the Science and Technology of Carbon Nanotubes and Their Composites: A Review." *Composites Science and Technology* 61 (2001): 1899-912.

Varanasi, Kripa, Tao Deng, Pramod Chamarthy, Shakti Chauhan, Peter De Bock, Ambarish Kulkarni, Gary Mandrusiak, Brian Rush, Boris Russ, Lauraine Denault, Stanton Weaver, Frank Gerner, Quinn Leland, and Kirk Yerkes. *Nanostructures for High Thermal Conductivity Substrates*. Tech. Cambridge, MA, Nisakayuna, NY, Cinncinnati, OH, Dayton, OH: Massachusetts Institute of Technology, GE Global Research Center, University of Cinncinnati, Air Force Research Lab, 2008.

Vasiliev, L.L. "Micro and miniature heat pipes – Electronic component coolers." *Applied Thermal Engineering* 26 (2008): 266-73. Print.

Wilson, Mick, Kamali Kannangara, Geoff Smith, Michelle Simmons, and Burkhard Raguse. *Nanotechnology Basic Science and Emerging Technologies*. Boca Raton, Fla: Chapman & Hall/CRC, 2002.

Xiaowei, Luo, Robin Jean-Charles, and Yu Suyuan. "Effect of temperature on graphite oxidation behavior." *Nuclear Engineering and Design* 227 (2004): 273-80.

Zhang, K., Y. Chai, M.M.F. Yuen, D.G.W. Xiao, and P.C.H. Chan. "Carbon nanotube thermal interface material for high-brightness light-emitting-diode cooling." *Nanotechnology* 19 (2008). Print.